Simulation of Matrix/Fracture Interaction in Low-Permeability Fractured Unconventional Reservoirs

D. Y. Ding and **N. Farah***, and **B. Bourbiaux,** IFP Energies Nouvelles;
Y.-S. Wu, Colorado School of Mines; and **I. Mestiri,** IFP Energies Nouvelles

Summary

Unconventional reservoirs, such as shale-gas or tight oil reservoirs, are generally highly fractured (including hydraulic fractures and stimulated and nonstimulated natural fractures of various sizes) and embedded in low-permeability formations. One of the main production mechanisms in unconventional reservoirs is the flow exchange between matrix and fracture media. However, because of extremely low matrix permeability, the matrix/fracture exchange is very slow and the transient flow may last several years to tens of years, or almost the entire production life. The commonly used dual-porosity (DP) modeling approach involves a computation of pseudosteady-state matrix/fracture transfers with homogenized fluid and flow properties within the matrix medium. This kind of model clearly fails to handle the long-lasting matrix/fracture interaction in very-low-permeability reservoirs, especially for multiphase flow with phase-change problems. Moreover, a DP model is not adapted for the simulation of matrix/fracture exchange when fractures are described by a discrete-fracture network (DFN). This paper presents an embedded discrete-fracture model (EDFM) dependent on the multiple-interacting-continua (MINC) proximity function to overcome this insufficiency of the conventional DP model.

Introduction

Unconventional tight oil or shale-gas reservoirs require stimulation by means of hydraulic fracturing to create fracture networks for profitable exploitation. The injection of a high-pressure fluid induces new channels or fractures in the rock and enhances the ultimate recovery. This operation also induces shear failure of the pre-existing natural fractures in shale formations, which results in natural-fracture opening and propagation, and in the creation of an extensive, interconnected flowing network (Delorme et al. 2013). This complex multiscale fracture network, including hydraulic and stimulated/nonstimulated natural fractures, together with the characteristics of extremely low-permeability formation, results in a complex multimedium reservoir and entails difficulties in the simulation of shale-gas or tight oil production (Mirzaei and Cipolla 2012; Wu et al. 2014).

There are several types of approaches to stimulate fractured reservoirs. Single-porosity models with very fine grids are used as reference models to discretize the fractures and the surrounding matrix medium. Although such models are accurate, they require extensive central-processing-unit (CPU) time and are inapplicable to field cases. Instead, fractured reservoir studies are usually performed on DP models where the fractured medium is represented as a continuum. DP-model cells incorporate equivalent fracture-medium properties, and transfers between fracture and matrix media (denoted as interporosity transfer) are computed to simulate local matrix/fracture interactions at cell scale. The DP model is conceptually simple and computationally efficient, but the interporosity-flow computation is not very accurate. To improve the conventional DP approach, Pruess and Narasimhan (1985) proposed the MINC method, which subdivides the matrix medium according to the distance from the fractures.

On the other hand, DFMs have received great attention to model realistic reservoir-fracture networks (Sarda et al. 2002; Hyman et al. 2015; Fourno et al. 2016). The DFM models that explicitly discretize all types of fractures, including hydraulically induced and stimulated and nonstimulated natural fractures, are considered accurate for conventional fractured-reservoir modeling, but involve too many unknowns and often intractable numerical systems to solve. Karimi-Fard et al. (2004) and Matthäi et al. (2005) developed DFMs using an unstructured control-volume formulation, in which the rock matrix is modeled by 3D polyhedral cells and the fracture network is represented by a subset of the 2D interfaces separating grid cells. The physical domain is discretized using unstructured grids. However, these models cannot practically be used to simulate natural fractures because of the prohibitive associated computational cost. Moreover, generation of such a grid for an arbitrary fracture network can be a substantial challenge.

To overcome the limitations related to a high number of unknowns and CPU time while maintaining solution accuracy, considerable efforts were recently dedicated to the development of hybrid approaches. Lee et al. (2001) and Li and Lee (2008) proposed a hierarchical fracture model to model fluid flow from naturally fractured reservoirs by taking into account multilength fractures. Their concept consists of explicitly discretizing long conductive fractures as major fluid conduits while short and medium fractures are homogenized, leading to a higher effective matrix permeability. The long conductive fractures are modeled with the EDFM approach. Using this concept, various EDFMs were tested and studied in the literature (Hajibeygi et al. 2011; Moinfar et al. 2011; Jiang et al. 2014; Norbeck et al. 2014; Xu et al. 2016). These models do not rely on unstructured grids to conform to the geometry and location of the fracture network, and they can significantly reduce CPU time for fluid-flow simulations of naturally fractured reservoirs. Hajibeygi et al. (2011) used the EDFM in a multiscale framework. Moinfar et al. (2013) implemented the EDFM, by preprocessing the input data, into a conventional reservoir simulator. Norbeck et al. (2014) used EDFM to develop an integrated framework where fracture networks can also grow and propagate according to the change in stress state. Thanks to EDFM, they do not need to regrid the model during the dynamic simulation.

In contrast with conventional reservoirs, unconventional shale-gas/tight oil reservoirs are characterized by extremely low matrix permeabilities. One of the main challenges in unconventional-shale-reservoir simulations is the flow transfer between matrix and fracture media. When matrix blocks have a large size, the traditional approach for simulating matrix/fracture transfers results in large errors in

* now with Lebanese American University

This paper (SPE 182608) was accepted for presentation at the SPE Reservoir Simulation Conference, Montgomery, Texas, USA, 20–22 February 2017, and revised for publication. Original manuscript received for review 2 March 2017. Revised manuscript received for review 26 October 2017. Paper peer approved 9 November 2017.

the prediction of field production. This is because it may take years to reach a pseudosteady-state flow regime in the matrix medium, because of the extremely low matrix permeability. A DP model, which computes an average pressure on a large matrix block, cannot describe the detailed pressure variation in the near-fracture zones.

Using the MINC approach is a solution for improving the accuracy for matrix/fracture-interaction computation in low-permeability reservoirs. MINC was originally developed to model heat and multiphase fluid flow in fractured porous media (Pruess and Narasimhan 1985). This concept is able to describe gradients of pressures, temperatures, or concentrations near the matrix surface and inside the matrix by further subdividing individual matrix blocks into 1D or multidimensional strings of nested meshes. Therefore, the MINC method treats interporosity flow in a fully transient manner by computing the gradients that drive interporosity flow at the matrix/fracture interface. As a result, the MINC model in general provides a better numerical approximation for fracture/matrix interactions than does the double-porosity model. This kind of method was applied to various studies of fractured reservoirs (Wu and Pruess 1988; Farhadinia and Delshad 2010). It was also investigated by Ding et al. (2014b) for the single-phase shale-gas simulations and by Farah et al. (2015) to study the fracturing-fluid-induced formation damage. A similar approach called multiple subregion was also proposed by Gong et al. (2006) and reviewed by Fumagalli et al. (2016) to treat the interporosity flow.

Jiang et al. (2014) and Jiang and Younis (2016) applied the MINC approach to the EDFM. Using the hierarchical approach, Jiang et al. (2014) and Jiang and Younis (2016) homogenized short/low-conductivity fractures, and used an MINC approach to simulate exchange between the matrix and the homogenized fracture media. Equivalent block sizes, which correspond to the effective fracture spacings in the *x*-, *y*-, and *z*-direction, are determined on each simulation gridblock, and the matrix medium is then subdivided into nested volumes with the MINC to handle matrix/fracture interaction. However, the detailed fracture-network geometry is not taken into account in the MINC subdivision.

Farah and Ding (2016) proposed an EDFM dependent on the MINC proximity function (EDFM-MINC) to improve the modeling of matrix/fracture interaction. The concept of the MINC proximity function was illustrated by Pruess and Karasaki (1982), but was not implemented. In this paper, the MINC proximity function is applied to multiscale fractures by computing the distance between the matrix element and all discrete fractures within each cell. Therefore, the fracture geometry and location are taken into account using the proximity function, and all fractures, including high-conductivity hydraulic fractures and homogenized stimulated/nonstimulated natural fractures, are considered in the matrix/fracture interaction. This approach is within the scope of a triple-porosity model, where the propped fractures, especially hydraulic fractures, are explicitly discretized and other fractures are homogenized. In this paper, we present some improved techniques to ameliorate the transmissibility computation for the EDFM-MINC approach. In particular, an integral-represented pressure distribution is used for the transmissibility calculation in the vicinity of hydraulic fractures. The connections between stimulated-reservoir-volume (SRV) and non-SRV cells are also adapted to the presence of MINC subdivisions in SRV cells.

The EDFM-MINC is particularly useful for the simulation of multiphase flow with phase-change problems. For example, in a tight oil reservoir, when the fracture pressure drops to less than the bubblepoint, gas starts to appear in the matrix formation near the fracture faces. The MINC method is suitable to simulate this kind of phenomena, which cannot be handled with a standard DP approach. Some numerical examples are presented to compare the EDFM-MINC approach, the DP model, and a fine-mesh single-porosity model with explicitly discretized fractures, which is considered as the reference solution. Both tight oil and shale gas with phase-change problems are investigated. The results show that the DP model is not suitable for the simulation of low-permeability unconventional reservoirs, and the proposed EDFM-MINC approach greatly improves the accuracy. Using the MINC-based approach, a compromise between simulation accuracy and CPU time is found.

Mathematical Model

We present in the following the governing equations for three-phase, multicomponent flow with a DP approach. The mole conservation for each component c in a DP/dual-permeability system is expressed per unit bulk volume of the reservoir as

$$\frac{\partial}{\partial t}\left[\phi^f \sum_p \left(\rho_p^f C_{cp}^f S_p^f\right)\right] + \text{div}\left[\sum_p \left(\rho_p^f C_{cp}^f \vec{u}_p^f + \vec{J}_{cp}^f\right)\right] - \sum_p Q_{cp}^{mf} - \sum_p \rho_p^f C_{cp}^f q_p^f = 0, \quad \ldots\ldots (1)$$

and

$$\frac{\partial}{\partial t}\left[\phi^m \sum_p \left(\rho_p^m C_{cp}^m S_p^m + v_{sg}\right)\right] + \text{div}\left[\sum_p \left(\rho_p^m C_{cp}^m \vec{u}_p^m + \vec{J}_{cp}^m\right)\right] + \sum_p Q_{cp}^{mf} - \sum_p \rho_p^m C_{cp}^m q_p^m = 0, \quad \ldots\ldots (2)$$

where the superscript f refers to the fracture and the superscript m to the matrix, the subscript p ($p = w, o, g$) refers to the phase water, oil or gas; ϕ^m and ϕ^f are the matrix and fracture porosity, respectively; C_{cp}^M (medium $M = f$ or m) is the mole fraction of the component c in phase p; S_p^M ($M = f$ or m) is the saturation of the phase p; ρ_p^M is the mole density of phase p; v_{sg} corresponds to the gas-sorption term that appears only in the gas-component-conservation equation in the matrix medium; $\vec{u}_p^M$ is the velocity of phase p in medium M; and $\vec{J}_{cp}^M$ is the molecular diffusion and dispersion flux of component c in phase p in medium M. In addition, q_p^M is the sink/source term of phase p per unit volume of formation in medium M, and Q_{cp}^{mf} is the matrix/fracture-transfer rate of component c in phase p per unit bulk volume of reservoir.

The phase velocity is expressed with Darcy's law in both the matrix and the fracture media with

$$\vec{u}_p^M = -k_M \frac{k_{rp}^M}{\mu_p^M} \text{grad}\left(\Phi_p^M\right), \quad \ldots\ldots (3)$$

and

$$\Phi_p^M = P_p^M - \rho_p^M g Z, \quad \ldots\ldots (4)$$

where $M = f$ or m represents the fracture or the matrix medium; Z is depth (positive, increasing downward); g is the algebraic value of gravitational-acceleration projection on the z-axis; k is the absolute permeability; P_p the pressure of phase p; μ_p is the viscosity of phase p; and k_{rp} is the relative permeability of phase p.

In a DP approach, the DFN is homogenized. In particular, we need the equivalent permeability and porosity in the homogenized fracture medium. The MINC method can be considered as a generalization of the DP approach. This method treats the interporosity flow inside the matrix media in a fully transient way for the matrix/fracture exchange.

For the single-porosity model, only Eq. 2 is considered. The absolute permeability can be either the matrix permeability or fracture permeability according to the considered location or the simulation cell. To build a reference solution with the single-porosity model, very fine meshes are used for the discretization of the matrix medium, and the fractures are explicitly discretized through their intersect nodes. The flow exchange between a matrix cell and a fracture node is computed using the method described in Sarda et al. (2002).

In a reservoir study, it is difficult to use a finely meshed single-porosity model by explicitly discretizing all the fractures because of the large number of grid cells and high CPU time. Using the EDFM-MINC approach is a solution. According to the EDFM concept, we explicitly discretize only highly conductive hydraulic fractures, and all other fractures are homogenized. In the SRV, the EDFM-MINC is used to simulate on one side the interaction between the homogenized fracture medium and the matrix medium using the MINC proximity function, and on the other side the interaction between the homogenized fracture medium and the discrete hydraulic fractures.

Numerical Method and Simulation Approach

The system of equations (Eqs. 1 through 4) is discretized in space using a control-volume method, where time discretization is performed using a backward, first-order, finite-difference scheme. The control-volume method is very flexible for handling the interactions between various kinds of continua. For example, the volumetric exchange rate of phase p between two grid cells is given by **(Fig. 1)**

$$F_{p,ij} = \lambda_{p,ij} T_{ij} (\Phi_{p,j} - \Phi_{p,i}), \quad \ldots\ldots (5)$$

where T is the transmissibility between two grid cells i and j, and $\lambda_{p,ij} = \frac{k_{rp}}{\mu_p}$ is the mobility term of phase p. The rate of mole transfer between matrix and fracture media in the dual-porosity model in phase p is computed per unit bulk volume as

$$Q_p^{mf} = \lambda_p^{mf} \rho_p^M k_m \sigma (\Phi_p^m - \Phi_p^f), \quad \ldots\ldots (6)$$

where σ is the shape factor. If the block dimensions are known, the following shape factor is used for the 2D matrix/fracture exchange:

$$\sigma = \frac{10}{a^2} + \frac{10}{b^2}, \quad \ldots\ldots (7)$$

where a and b are the block sizes in the x- and y-direction, respectively. This shape factor is close to that given by Lim and Aziz (1995) for single-phase exchange, and by Bourbiaux et al. (1999) for both single-phase and two-phase transfers. The accuracy of the discretized scheme depends greatly on the transmissibility and the shape-factor formulation. This is particularly true in low-permeability unconventional reservoirs.

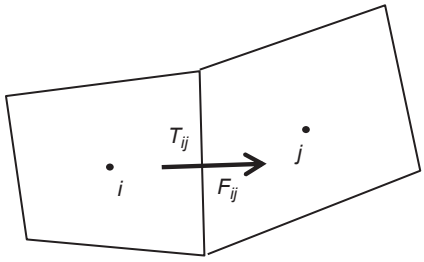

Fig. 1—Flux approximation in the control-volume method.

One of the key issues in numerical modeling for unconventional shale-gas or tight oil reservoirs is the handling of fluid-flow exchanges in the presence of a complex-fracture network, including hydraulic and propped fractures and stimulated/nonstimulated natural fractures **(Fig. 2).** All these fractures are connected to each other, leading to a very complex DFN. The EDFM approach takes into consideration three media: discrete high-conductivity hydraulic fractures; homogenized fracture medium for the stimulated/nonstimulated natural fractures; and matrix medium. In the SRV, all three media are considered. Outside the SRV, only a single-porosity approach is used. For an EDFM, the flow-exchange term can always be written in the form of Eq. 5 or Eq. 6, but the transmissibility T depends on the fracture geometry and on the permeability of the interacting medium in the cells under consideration.

In this paper, we classify the fractures, generated by a geostatistical model, depending on conductivity criteria. Hydraulic fractures and propped stimulated fractures are usually highly conductive, and will be explicitly discretized because of their very important role in the production. Other fractures are homogenized. It must be mentioned that among all interactions, the modeling of flow exchange between matrix and fracture is extremely important because of the ultralow matrix permeability. On the other hand, it is assumed that no flow occurs between two matrix cells in the SRV.

Flow Within the Discrete Network of Hydraulic Fractures. Highly conductive fractures, such as hydraulic fractures, have a more-dominating influence on fluid flow than short and medium fractures. These highly conductive fractures are explicitly discretized and modeled using fracture nodes. Each intersection of two (or more) high-conductivity fractures (black lines in **Fig. 3**) constitutes a fracture node (red node in Fig. 3). A fracture volume and an exchange surface area are assigned to each fracture node to compute fluid flow inside the high-conductivity fractures (Khvoenkova and Delorme 2011).

Exchange Between High-Conductivity Fractures and the Homogenized Fracture Medium. Most DFMs, including EDFMs, assume a linear pressure distribution around fractures (Lee et al. 2001; Moinfar et al. 2011; Farah and Ding 2016), and they use a linear

approximation to compute flow exchange between a discrete fracture and a continuous medium. Under this assumption, the transmissibility T_{kj} between a homogenized fracture cell k and a hydraulic-fracture node j is given by

$$T_{kj}^{fF} = k_{fk} \frac{A_{kj}}{< d_{kj} >}, \quad (8)$$

where k_{fk} is the equivalent permeability of the cell k, A_{kj} is the exchange surface area between the hydraulic fracture attached to node j and cell k, and $< d_{kj} >$ is the average distance between cell k and the hydraulic fracture associated with node j.

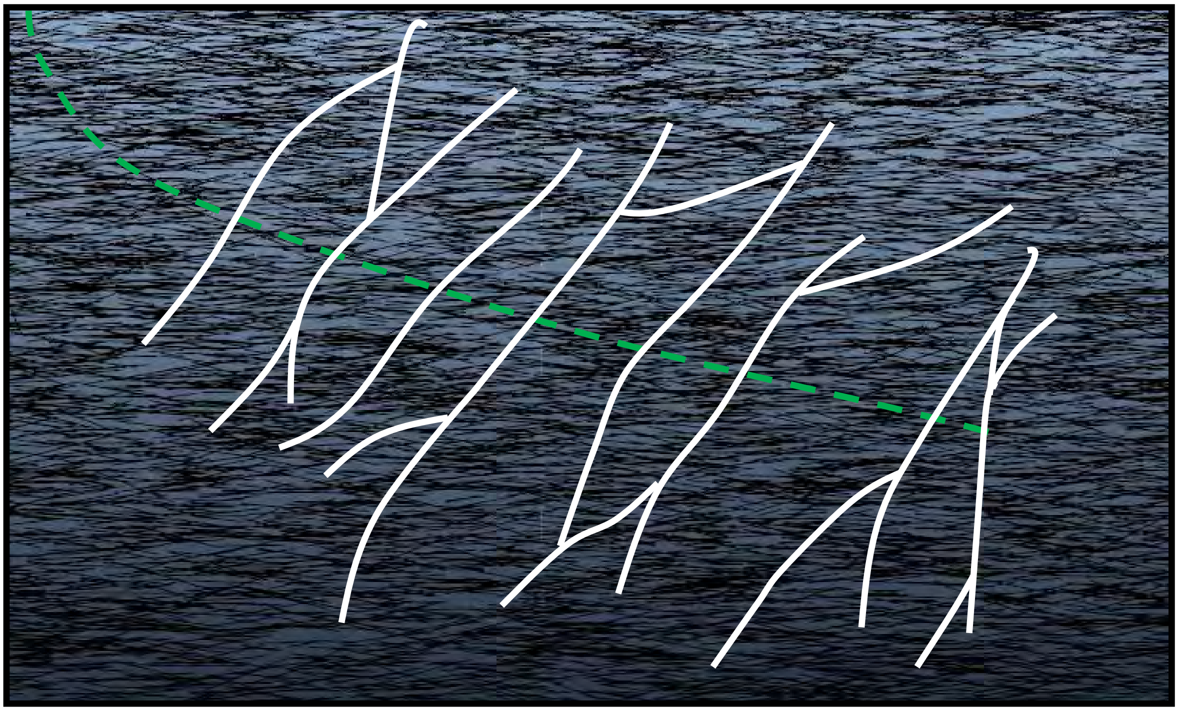

Fig. 2—Illustration of the hierarchical model with multiscale fractures: high-conductivity hydraulic fractures (white lines) and low-conductivity induced and natural fractures (black lines).

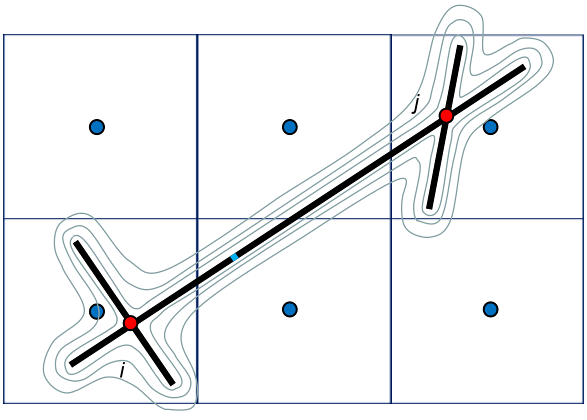

Fig. 3—Pressure distribution (isopressure lines) around fractures.

However, the assumption of linear-pressure distribution is not always true, especially near the fracture extremities and the fracture-intersection zones (Fig. 3). The isopressure lines are affected by the presence of other fractures and the extremity effects.

To get a more-realistic pressure distribution around fractures, Ding et al. (2014a) proposed to use an integral method to represent isopressure distribution in the near-fracture field for a steady-state flow. The integral representation gives a suitable description for both the linear isopressure line near the middle of an isolated fracture and curved isopressure lines near the fracture ends or intersections. Once the pressure field around the hydraulic fracture is known, the transmissibility between the homogenized fracture cell k and the hydraulic-fracture node j can be identified by Darcy's law with the formula

$$T_{kj}^{fF} = \left| \frac{\mu F_{kj}}{P_{f,k} - P_{F,j}} \right|, \quad (9)$$

where $P_{F,j}$ is the pressure on the node j; $P_{f,k}$ is the average pressure on the homogenized fracture cell k; μ is the fluid viscosity; and F_{kj} is the flow rate from the cell k to the fracture node j through the exchange surface A_{kj}. All these variables are computed using the integral method (Ding et al. 2014a). Because the pressures and the flux in Eq. 9 are computed under a steady-state flow regime, the transmissibility remains constant during the dynamic simulation.

Flow Within the Homogenized Fracture Medium. In general, the transmissibility between two homogenized fracture cells is calculated as

$$T_{ij}^{f} = A_{ij}\frac{k_{fi}k_{fj}}{d_i k_{fj} + d_j k_{ij}}, \quad (10)$$

where A_{ij} is the exchange surface between the two homogenized cells i and j, k_{fi} and k_{fj} are the homogenized fracture permeabilities on the cells i and j, and d_i and d_j are the distance from the cell center to the exchange surface **(Fig. 4).** However, Eq. 10 is not suitable for flow simulation near highly conductive hydraulic fractures. Let us consider a hydraulic fracture that intersects one of two neighboring homogenized fracture cells (the red line in Fig. 4). If we use Eq. 10 for the transmissibility calculation, the fluid in cell i will be driven first to the center of cell j and then back to the hydraulic fracture. This approach underestimates the flow rate between cell i and the hydraulic fracture, if they are quite close, as shown in Fig. 4.

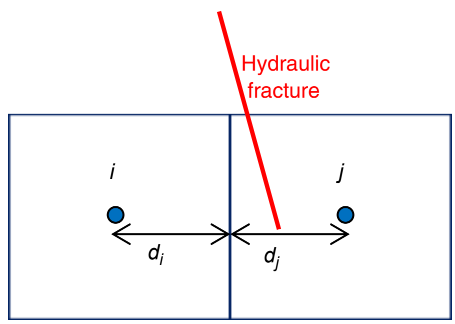

Fig. 4—Transmissibility between two homogenized fracture cells.

To take into account the effect of the presence of hydraulic fractures on the fluid flow in the homogenized medium, we propose to again use the integral representation for transmissibility computation. If one of the homogenized cells intersects with a conductive fracture, it is not convenient to represent the pressure of this cell at its cell center. Instead, the average cell pressure can be represented using an integral formula (Ding et al. 2014a). In this case, we propose to determine the transmissibility between these two cells through an identification from Darcy flow by

$$T_{ij}^{f} = \left|\frac{\mu F_{ij}}{P_{f,i} - P_{f,j}}\right|, \quad (11)$$

where $P_{f,i}$ and $P_{f,j}$ are the average fracture pressures of cells i and j, given by the integral formulas, and F_{ij} is the flow exchange between these two cells, also calculated from the integral formula, which corresponds to the pressure-normal directive on the interface between the two cells.

If both considered homogenized cells do not intersect any discretized conductive fracture, we use the pressures defined at the center of the grid cells and the transmissibility is determined with the linear approach of Eq. 10.

These two different transmissibility-computation methods—the linear approach with Eqs. 8 and 10 and the integral-based approach with Eqs. 9 and 11—will be compared later.

Exchange Between Matrix Medium and Fractures. One of the key issues in the modeling of a low-permeability fractured reservoir is the matrix/fracture interaction. To improve the accuracy, the MINC concept is applied. The MINC method can be considered as a generalization of the DP concept. The main difference between the MINC method and a DP model is in the matrix/fracture exchange known also by "interporosity flow." The DP method simulates matrix/fracture exchange derived from pseudosteady-state flow, while the MINC method treats the problem entirely with a numerical approach in a fully transient way. In general, the MINC model provides a better numerical approximation for transient fracture/matrix interactions than a DP model.

The basic idea of the MINC is to subdivide a matrix cell according to the distance from the fractures. Although using an isopressure line for cell subdivisions might be more accurate for interporosity-flow simulation (Ding et al. 2014b; Cai et al. 2015), for simplicity, a generalization of this kind of approach to the EDFM is not discussed in this work. The choice of MINC subcell thicknesses is not discussed here, although it can be optimized to best follow the local evolution of pressure in the matrix medium, as shown by Famy et al. (2005) for a two-phase-flow transfer problem.

In the EDFM, a matrix cell may interact with all sorts of fractures, including both highly conductive hydraulic fractures and low-conductivity stimulated/nonstimulated natural fractures. All these interactions are modeled using the MINC approach. So, when we subdivide a matrix cell, the subcells are constructed by considering the distance to both hydraulic and connected natural fractures, as shown in **Fig. 5.** Because hydraulic-fracture nodes are not necessarily inside the considered matrix cell, for simplicity, we affect first all flow exchanges between matrix and fractures to the homogenized fracture cell, and then the homogenized cells exchange with hydraulic-fracture nodes. In other words, the modeling of matrix/fracture interaction takes into account all types of connected fractures, but the exchange between a matrix cell and hydraulic fractures is performed using a homogenized fracture cell in the numerical modeling. It must be mentioned that the equivalent permeabilities and porosities are determined with only the low-conductivity fractures, whereas the exchanges between matrices and fractures involve all sorts of fractures.

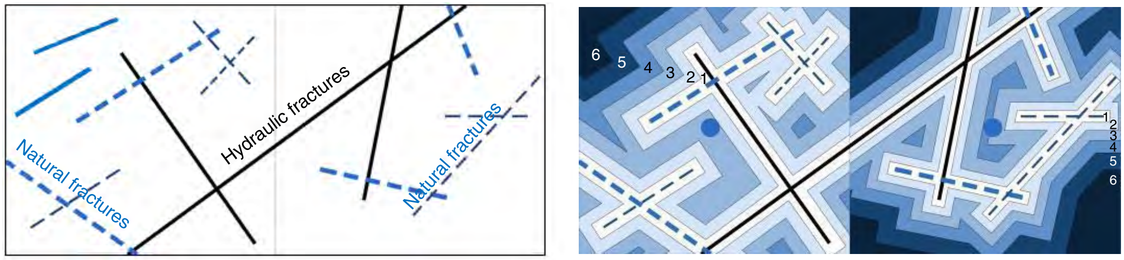

(a) A DFN (connected and isolated)

(b) Computing the MINC proximity function for a MINC6 model

Fig. 5—Illustration of the MINC method.

To subdivide a matrix cell, a number of points are randomly launched inside the cell. The distance between a random point within the matrix and all connected fractures inside the cell is calculated. Thus, the histogram of random point distances to the fractures can be plotted. For example, **Fig. 6a** shows a histogram where distances are grouped by intervals of 0.25 ft for 1,000 points launched in a square cell. Fig. 6b is the cumulative distribution function of these 1,000 points (denoted ζ) with respect to the distance from the fractures.

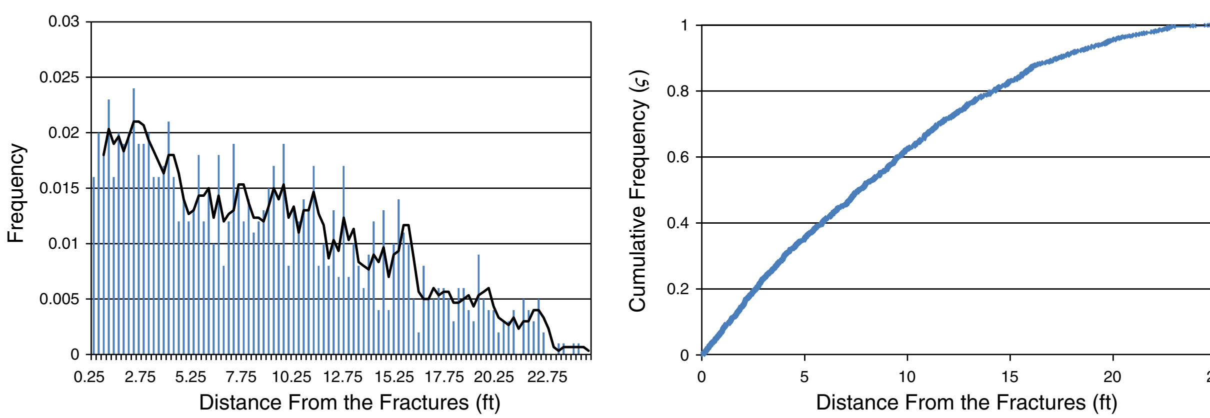

(a) Histogram

(b) Cumulative distribution function

Fig. 6—Illustration of an example representing the point distribution vs. the distance from the fractures.

Using the distribution function, we can subdivide a matrix cell according to the distance from the fractures. Let $d_0 = 0 < d_1 < d_2 < \ldots < d_n = d_{\max}$ be a discretization on the interval $[0, d_{\max}]$ with $d_{\max}$ being the maximum distance from the cell to the fractures. The ith MINC subblock is constructed by the volume of matrix cell with a distance to the fractures comprised between d_{i-1} and d_i. The first MINC subblock connects to the homogenized fracture medium, and the transmissibility T_j^{fm} between this first MINC subdivision and a fracture cell j is given by

$$T_j^{fm} = 2\frac{k_{mj}}{d_1}A_j^{fm}, \quad (12)$$

where A_j^{fm} is the area of the fracture surface in the cell j, and k_{mj} is the matrix permeability of the cell j. The transmissibility between the two subcells i and $i+1$ is given by

$$T_i^m = \frac{A_i K_m}{d_{i+1} - d_i}, \quad (13)$$

where A_i is the area of the interface between these two subcells. This area corresponds, in fact, to the derivative of the cumulative volume of matrix with respect to the distance from the fractures. The cumulative volume of matrix within a given distance from the fractures in the cell is obtained as the product of the cumulative random-points fraction ζ (Fig. 6b) and the total bulk volume of the matrix cell. Therefore, the exchange area between the two MINC matrix subdivisions i and $i+1$ can be approximated using a finite-difference approach:

$$A_i = \frac{V_{i+1} - V_i}{d_{i+1} - d_i} = \frac{\mathrm{d}\varsigma}{\mathrm{d}x}V_{\text{cell}}, \quad (14)$$

where V_i is the cumulative volume of matrix within a distance x from the fractures equal to d_i, and V_{cell} is the cell volume.

For a general fracture network, the DP model is considered as a particular case of the MINC method with only one matrix subdivision. In that case, the shape factor is computed with Eq. 12.

Exchange Between SRV and Non-SRV. The contribution from the zone outside SRV is not negligible, especially for non-SRV cells very close to the SRV. Therefore, it is necessary to correctly model the fluid-flow exchanges between SRV and non-SRV zones.

Fig. 7 shows the connection between a SRV cell i and a non-SRV cell j. The cell i is subdivided by the MINC proximity function according to the distances from the fractures of that cell. Therefore, the connections of cell i with the neighboring cell j are computed by means of the MINC subcells of cell i that are found at the interface between the two cells. The transmissibility between the kth MINC subdivision of cell i and the non-SRV cell j is calculated as

$$T_{ij}^{k} = \frac{k_{mi}k_{mj}}{d_j k_{mi} + d_i^k k_{mj}} A_{ij}^{k}, \quad (15)$$

where k_{mi} and k_{mj} are the matrix permeabilities of cells i and j, respectively; A_{ij}^{k} is the exchange area between the cell j and the kth MINC subdivision of cell i; d_j is the distance from the center of cell j to the exchange surface; and d_i^k corresponds to the difference between the average distance d_A^k from the k exchange area A_{ij}^{k} to the fractures and the average distance d_M^k of the MINC subdivision k toward the fractures:

$$d_i^k = \max(d_A^k - d_M^k, 0). \quad (16)$$

Note that we use only a positive distance; that is, if $d_i^k < 0$, then we define $d_i^k = 0$.

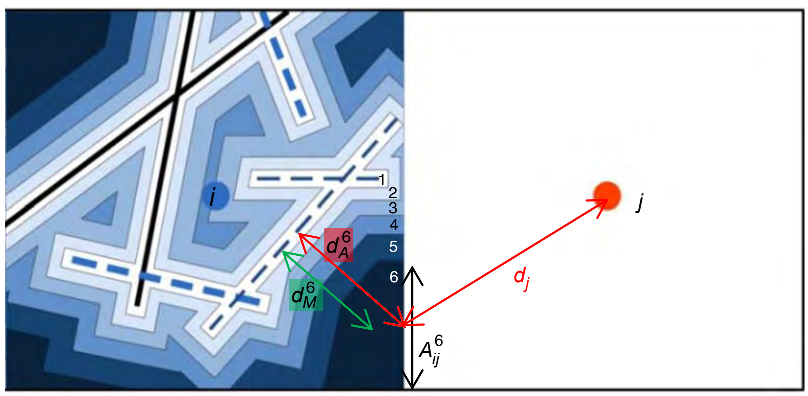

Fig. 7—Connection between SRV and non-SRV cell.

Numerical Example

In all the examples, the reference solution is obtained on a very fine mesh with a single-porosity approach in which all fractures are explicitly discretized. All examples are 2D cases, where the vertical direction is not discretized.

In the first example, we validate EDFM-MINC with a Warren and Root fracture network (Warren and Root 1963) for a single-phase gas flow. Then, we study phase-change problems for both tight oil and shale-gas/condensate problems. For the tight oil case, a black-oil model is used. Mobile water is assumed to be present in this reservoir. Therefore, it is a problem of three-phase flow. One of the issues for tight oil simulation is the matrix/fracture interaction with phase change near the fracture faces. For the retrograde shale-gas case, a compositional model is used. The simulation cases presented hereafter are focused on the predictive capacity of the MINC method for modeling matrix/fracture interaction.

Single-Phase Flow on a Regular Fracture Network. Shale-gas single-phase flow is considered on a Warren-and-Root-type fracture network to compare the EDFM-MINC and the DP model with the reference solution, which is obtained using a single-porosity model with very-fine-grid cells and explicit fracture discretization. The two types of transmissibility connections, dependent on the linear pressure and the integral-represented pressure distributions, are compared.

Consider an SRV of 1,050 × 1,000 × 300 ft, as shown in **Fig. 8.** Apart from the highly conductive hydraulic fractures, all other fractures are homogenized in the SRV and the MINC method is applied to subdivide the matrix medium using the distance from the fractures. The hydraulic fracture length is 300 ft (red solid line in Fig. 8), and the spacing of the natural-fracture network is 50 ft in both the x- and y-direction. **Table 1** summarizes the reservoir properties. A horizontal well is intersected at the middle of the hydraulic fracture (green point in Fig. 8), and it is assumed that the well production comes only through the hydraulic fracture. For the coarse grid simulation, the reservoir is discretized by 51 cells in the x-direction, 50 cells in the y-direction, and only one cell in the z-direction.

Because the fractures are regularly distributed and oriented to the grid-axis directions, we can accurately compute the equivalent permeabilities on the homogenized fracture medium. A MINC6 subdivision, which means that each matrix cell is subdivided by six subcells, is used for the EDFM-MINC approach. **Fig. 9** presents the cumulative gas production simulated with the EDFM-MINC, the DP model, and the single-porosity model over 16,000 days. For the EDFM-MINC model, two transmissibility formulas (linear-based and integral-based approaches) are compared. Obviously, the EDFM-MINC model provides a much better result than the DP model, and the integral-based transmissibility approach is more accurate than the linear-based transmissibility formula. The DP model greatly underestimates the gas production and is not suitable for fractured low-permeability reservoir simulations. Our EDFM-MINC shows the ability of predicting gas production from unconventional fractured gas reservoirs, whereas a DP model is inaccurate for such problems.

Now, let us consider the case where the SRV is not uniformly distributed in the whole simulation domain **(Fig. 10). Fig. 11** compares the cumulative gas production for the EDFM-MINC models with the two different transmissibility formulas and the reference solution (single-porosity model). Although all models provide satisfactory results, using the transmissibility dependent on the integral-based pressure distribution is more accurate than the one dependent on the linear-based pressure distribution. Our EDFM-MINC method is also suitable for simulations containing non-SRV zones.

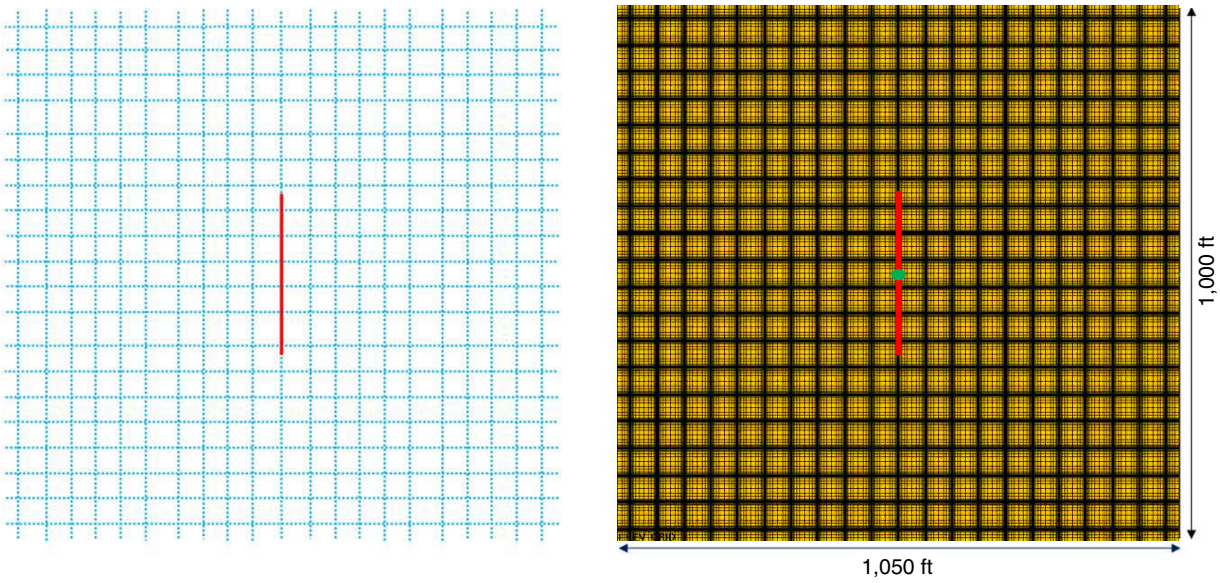

(a) A regular Warren-and-Root-type fracture network

(b) Explicit discretization of the fractures for the reference solution

Fig. 8—Illustration of the regular fracture distribution.

Property/Parameter	Value	Unit
Matrix permeability	0.0001	md
Hydraulic-fracture permeability	50	darcies
Induced-fracture permeability	200	md
Fracture width	0.01	ft
Induced-fracture width	0.001	ft
Reservoir net thickness	300	ft
Initial reservoir pressure	3,800	psi
Bottomhole well pressure	1,000	psi

Table 1—Reservoir properties for the regular-fracture-network simulation.

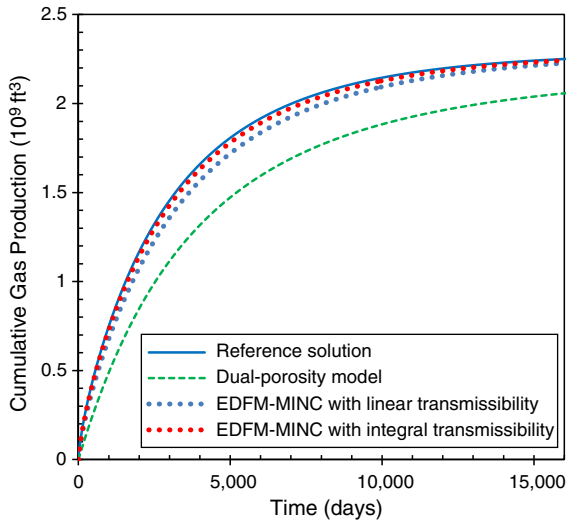

Fig. 9—Comparison of simulations on the regular fracture network.

Simulation of Phase Change in a Single Matrix Block. In this session, we study the matrix/fracture exchange for multiphase flow with phase change in a single matrix block. Consider a matrix block with an equal size of 100 ft in the x- and y-direction and surrounded by fractures, as shown in **Fig. 12.** The permeabilities are 2 darcies and 0.001 md, respectively, in the fracture and the matrix. The fracture width is 0.04 in. The matrix porosity is 0.05. We consider a tight oil case first and then a gas/condensate case.

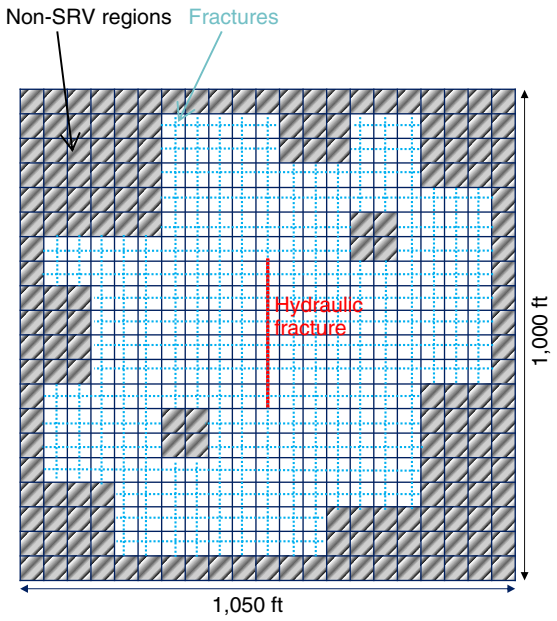

Fig. 10—Warren and Root fracture distribution with non-SRV regions.

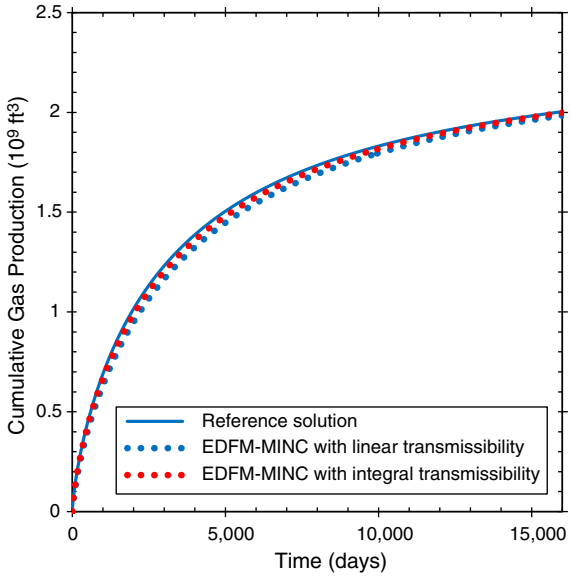

Fig. 11—Simulations with non-SRV regions.

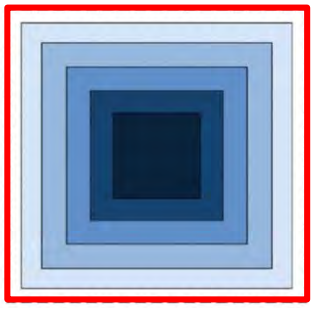

Fig. 12—Simulation on a single matrix block with MINC subdivisions.

To obtain the reference solution, a fine-grid simulation is performed with 217×217 grid cells in the x–y plane. The maximum cell size is 0.5 ft. The fracture is explicitly discretized with cells sized at 0.04 in. The near-fracture matrix cells are also very small, starting from size of 0.04 in., and increased logarithmically with 12 gridblocks until the maximum size is 0.5 ft. This fine-grid simulation is considered as the reference solution. For the DP simulation, only one matrix cell and one fracture cell are used, and the well is connected to the fracture cell. For the MINC approach, the matrix cell is subdivided according to the distances from the fractures (Fig. 12).

Tight Oil Simulation. For the tight oil case, a black-oil model is used. The initial reservoir pressure is 2,900 psi, and the bubblepoint pressure is 2,710 psi. The well bottomhole pressure (BHP) is imposed to 1,160 psi. The matrix block also contains mobile water with a saturation of 0.39, while the irreducible water saturation is 0.1. Because the fractures have small volume, high permeability, and linear relative permeabilities (X-curves), the well production on the medium- to long-term results should correspond to the matrix/fracture exchange.

Different MINC subdivisions (MINC6, MINC8, MINC12, and MINC16) are applied. The simulation results are compared with the fine-grid simulation on one side and the DP model on the other side. **Fig. 13** presents the cumulative oil and gas production. All MINC simulations provide satisfactory results, whereas the DP approach is not accurate, especially for the gas production. This can be explained by the phase change near the fracture face. **Fig. 14** presents the gas/oil ratio (GOR), which are very sensitive data. In this example, the solution GOR is 960 ft^3/bbl. For the DP model, because only one matrix grid cell is used, the cell pressure remains higher than the bubblepoint pressure at early times. Therefore, the GOR of the DP model in the beginning is very close to the solution GOR. For the fine-grid reference simulation or the MINC method, the grid cells near the fracture are small, and the pressures on these cells drop very quickly to lower than the bubblepoint pressure. This leads to higher GOR production at very early times. This high GOR corresponds to some field observations (Khvoenkova et al. 2015). Refining the MINC model (MINC8, MINC12, or MINC16) improves results if compared with the simulation of a coarse MINC model, such as MINC6. After 400 days, GOR simulated with MINC models starts to diverge from the reference solution. This is because the oil production is very low, and a small difference in oil production may lead to a strong GOR variation. **Fig. 15** presents the simulated oil- and gas-production rates. It shows that all MINC methods give quite satisfactory results at this scale. But from 400 days, the oil rate becomes very small and close to zero (less than 0.2 B/D), and so a small difference in oil rate could lead to a large variation in GOR. In our case, the relative differences in oil rate are large, which induce large GOR differences. Hence, comparison of long-term GOR in this example is not meaningful. Although all MINC subdivisions provide globally satisfactory results, increasing the number of matrix subdivisions does not always ameliorate the accuracy. In fact, with complex physics, such as a multiphase flow with phase change, the simulation results—especially GOR—are sensitive to the grid sizes near the fractures. Nevertheless, we noticed that the general trends are good.

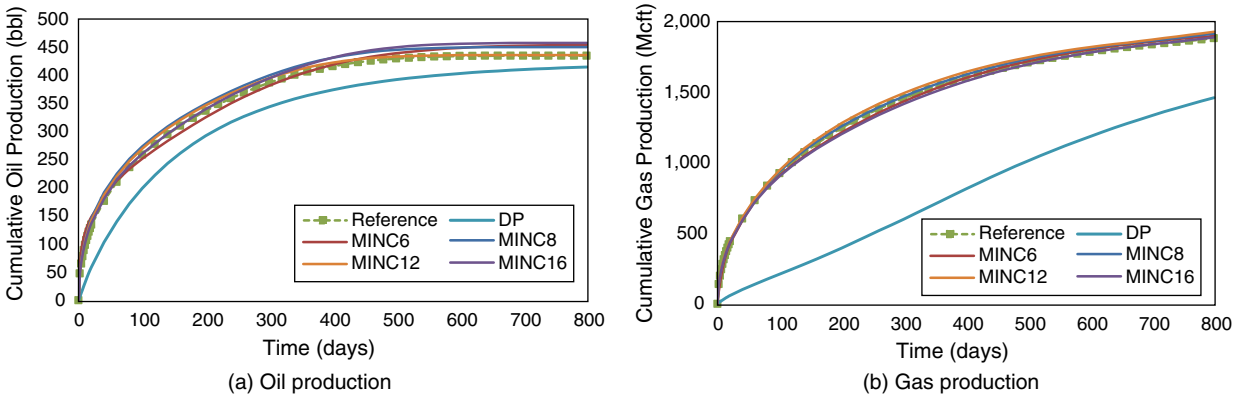

Fig. 13—Cumulative oil and gas production in the single-matrix-block simulation in the tight oil case.

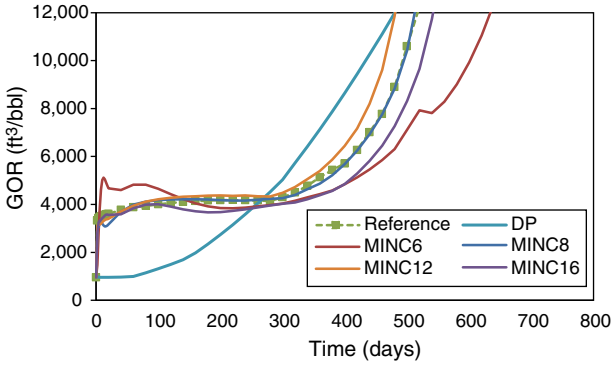

Fig. 14—GOR in the single-block simulation in the tight oil case.

Fig. 16 shows the pressure and gas saturation vs. the distance to the fractures simulated with previous models. The MINC method predicts profiles that are very close to the ones given by the fine-grid model, even with a limited number of subdivisions of the matrix medium, as considered in Fig. 16 (MINC6). Therefore, the MINC model can simulate the high production GOR from the fine-grid model because the MINC pressure near the fracture is correctly computed. **Fig. 17** compares cumulative water production. Again, the MINC approach gives reasonably accurate results, whereas the prediction of the DP model is not suitable.

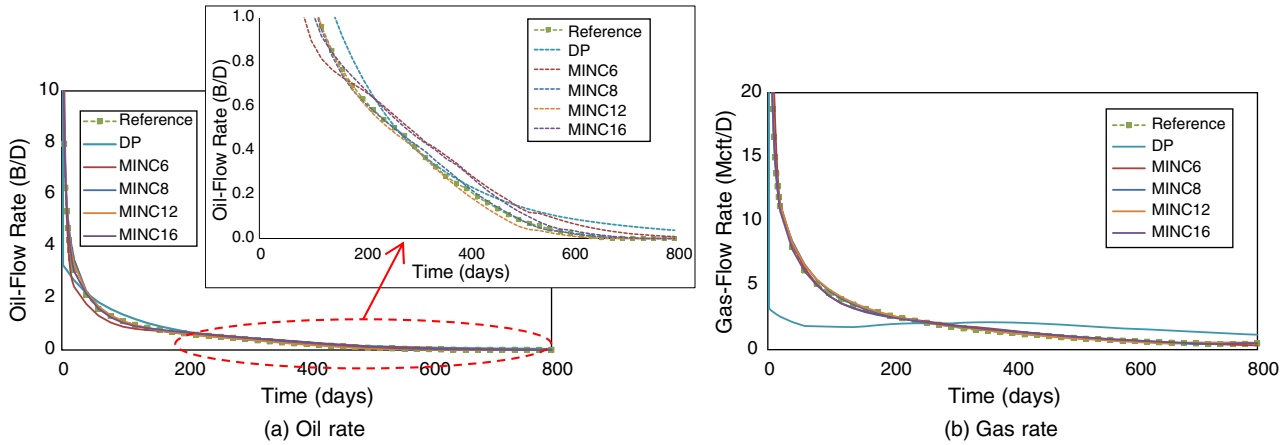

Fig. 15—Oil/gas-production rate in the single-block simulation in the tight oil case.

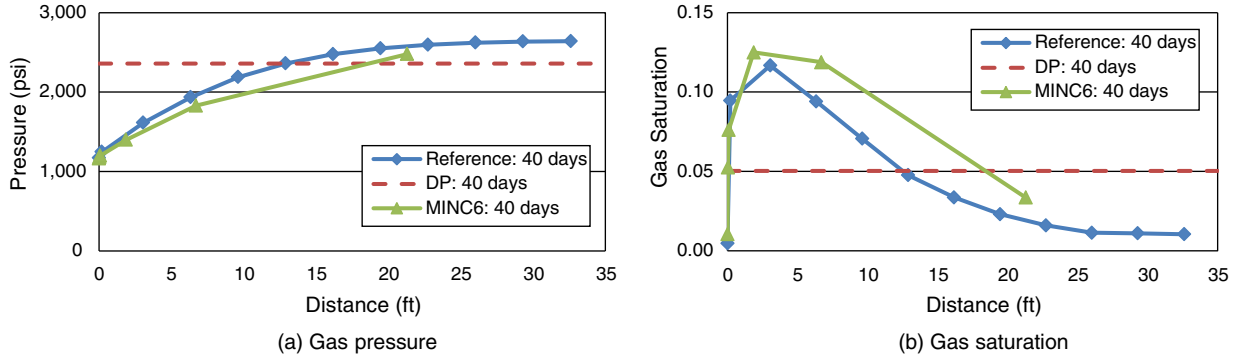

Fig. 16—Gas pressure and saturation vs. the distance from the fracture at 40 days.

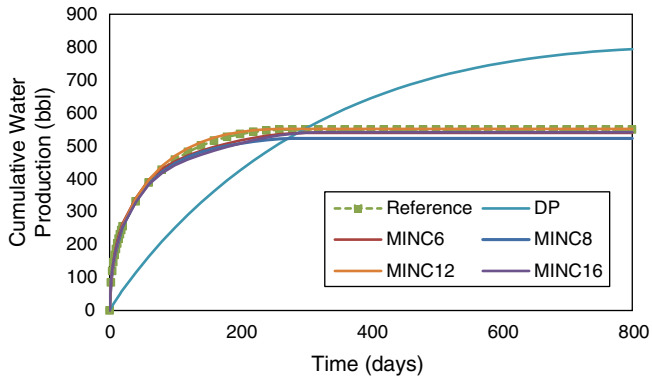

Fig. 17—Cumulative water production in the single-block tight oil simulation.

Now, we consider another test with a higher initial matrix pressure of 3,480 psi and a higher well BHP of 2,030 psi. **Fig. 18** presents the oil and gas production, and **Fig. 19** shows the produced GOR. Again, the MINC approach gives quite satisfactory results. In this test, the difference between the DP simulation and the reference solution is smaller because the initial pressure is much higher than the bubblepoint pressure, and for most of the time, the well effluent is a single oil phase or includes a very small amount of liberated gas. Because only a small volume of gas is present in the near-fracture zone, the GOR curves predicted by the fine-grid model or the MINC method are not as high as in the previous case.

Retrograde Shale-Gas Simulation. For this gas/condensate case, a compositional simulator is used. Eight components are presented in **Table 2.** This case is for a liquid-rich gas/condensate reservoir. In this test, the initial pressure is 6,000 psi and the well flowing pressure (fracture pressure) is 1,200 psi. The dewpoint pressure is approximately 3,000 psi. The main flow feature of gas/condensate systems is the dropout of a liquid-hydrocarbon phase within the pores of the reservoir rock as pressure falls to less than the dewpoint pressure. A condensate ring then builds up around the wellbore where the pressure gradient is the highest, leading to a gas-productivity decline.

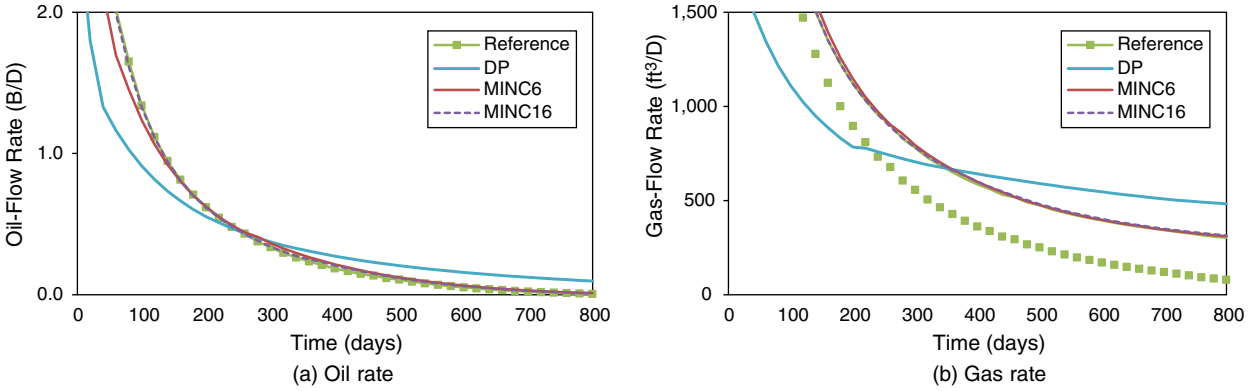

Fig. 18—Oil and gas production with a higher initial pressure.

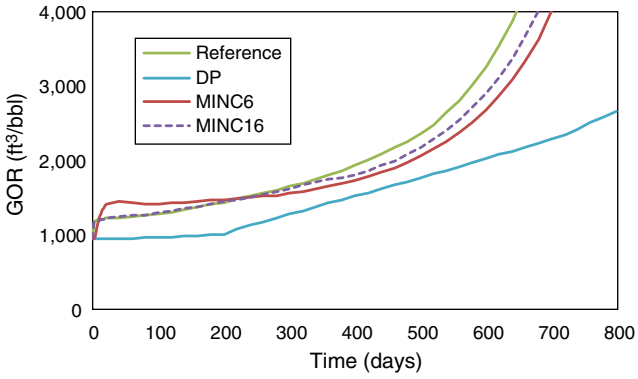

Fig. 19—GOR in the single-matrix-block simulation with a higher initial pressure.

Component	P_c (psi)	T_c (°F)	Acentric Factor	Molecular Weight	Mole Fraction (%)
CO_2	1,071.33	88.76	0.225	44.01	1.21
C_1	667.78	–116.62	0.013	16.043	65.99
C_2	708.34	90.07	0.0986	30.07	8.69
C_3	618.70	205.94	0.1524	44.097	5.91
$C_{4\text{-}6}$	514.93	346.84	0.2158	66.869	9.67
Pseudo 1	410.75	378.41	0.3123	107.779	4.745
Pseudo 2	247.56	598.34	0.5567	198.562	1.515
Pseudo 3	160.42	832.19	0.9169	335.198	0.33

Table 2—Gas composition.

As depletion continues, the condensate dropout occurs throughout the reservoir. The low mobility of condensate compared with that of gas, plus a possible capillary trapping, leads to an increase in the production GOR (gas/condensate) ratio, or a decrease of the condensate/gas ratio (CGR). That is, gas/condensate-fluid systems encounter two main issues: gas-productivity drop and a poor recovery of condensate. For fractured reservoirs, the management of these production issues requires an accurate prediction of condensate dropout within the matrix blocks, which are actually the main source of recovered fluids. For the studied case, a single set of conventional (immiscible) relative permeability curves was considered, although the low interfacial-tension conditions that sometimes prevail in the vicinity of the dewpoint pressure may affect these curves.

Fig. 20 shows the gas/condensate production for the reference solution, the DP model, and the MINC methods with six and 16 subdivisions. As in the tight oil case, the DP model highly underestimates the gas production in early time. **Fig. 21** presents the pressure vs. the distance from the fractures at different times (2, 20, and 200 days) for the reference solution and the DP model. Clearly, the matrix pressure in the DP model—that is, the average pressure of the matrix block—remains higher than the dewpoint pressure (approximately 3,200 psi) for a very long time, whereas the pressure near the fracture face drops very quickly with other models. So, the DP model produces much more condensate because no liquid drops out within the matrix block for more than 2 years. **Fig. 22** presents the CGR. For the DP model, CGR remains equal to the initial CGR of the single-phase fluid and starts to decrease only after 800 days, or the time at which the slowly decreasing average matrix-block pressure reaches the dewpoint pressure. In contrast, the reference model and the MINC-based models predict a very early drop in condensate production and CGR because of the matrix subgridding that allows condensation to rapidly take place near the fracture as the consequence of pressure dropping immediately to the fracture pressure there.

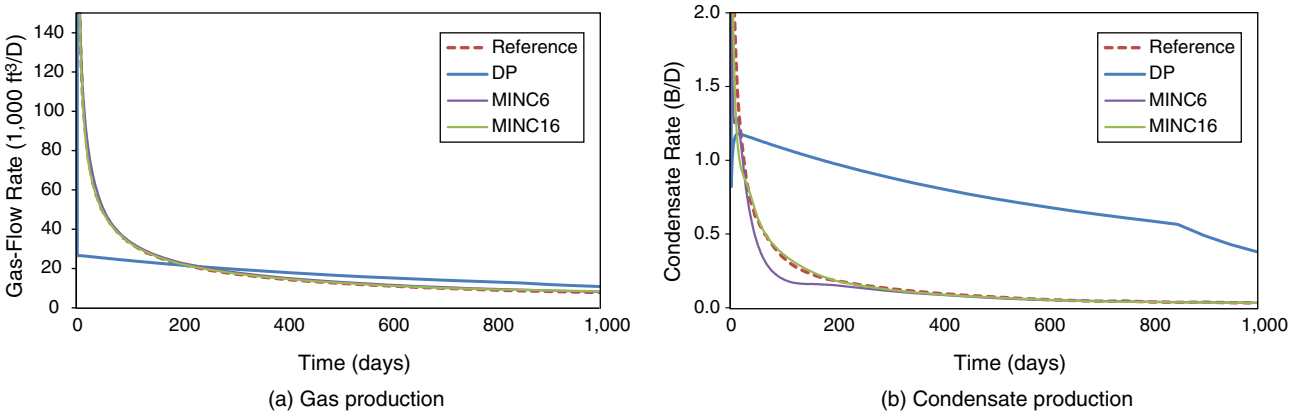

Fig. 20—Gas/condensate production in the single-block simulation in the shale-gas case.

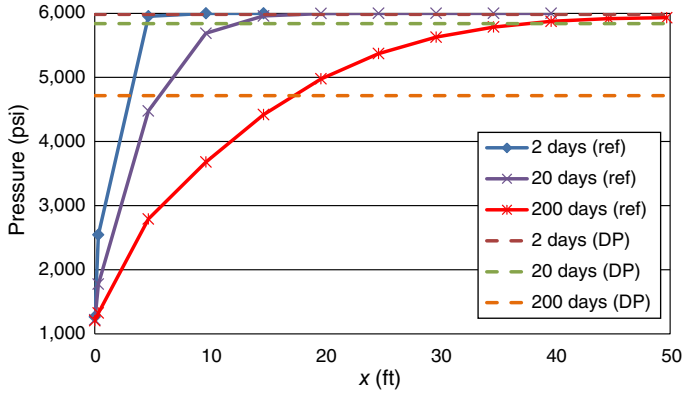

Fig. 21—Pressure variation as a function of distance from the fracture in the single-block simulation.

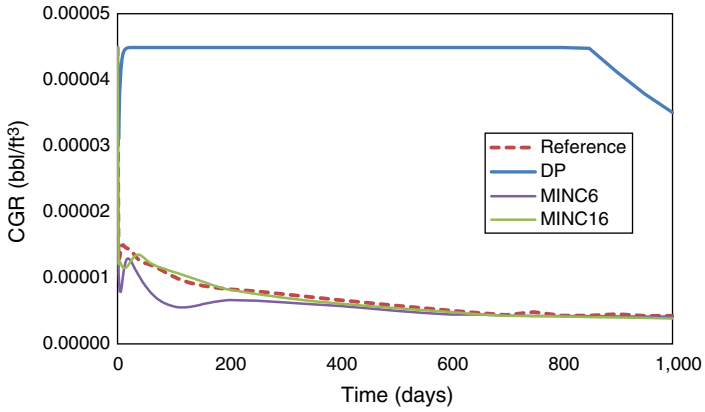

Fig. 22—CGR in the single-block simulation.

These simulation results show that the MINC method gives very satisfactory results for multiphase-flow simulations in fractured reservoirs thanks to an accurate prediction of phase-change effect on matrix/fracture transfers and reservoir production. This is a major limitation of DP models for their application to shale reservoirs.

A 2D Synthetic Case. Now, we consider a more-realistic synthetic case: a stimulated fracture network around a hydraulic fracture within a single reservoir layer, as shown in **Fig. 23.** We limit our simulations to a bounding box (or SRV) of $820 \times 1{,}800 \times 20$ ft. This reservoir contains two sets of natural fractures. One set of natural fractures is oriented with an average angle of 75° from the north to the northeast and has a mean length of 200 ft. The second set of fractures has an average orientation of 150° from the north to the southeast with a mean length of 400 ft. A hydraulic fracture oriented to the north is considered in the middle of this SRV, with a length of 1,480 ft, a width of 0.012 ft, and a permeability of 20 darcies. These two sets of natural fractures are stimulated by hydraulic fracturing and have a thickness varying from 0.004 to 0.005 ft and permeability from 300 to 400 md. In this example, we assume that natural fractures are not fully propped, even if they are stimulated. So, only the hydraulic fracture is explicitly discretized in the EDFM-MINC approach. The two sets of natural fractures are homogenized.

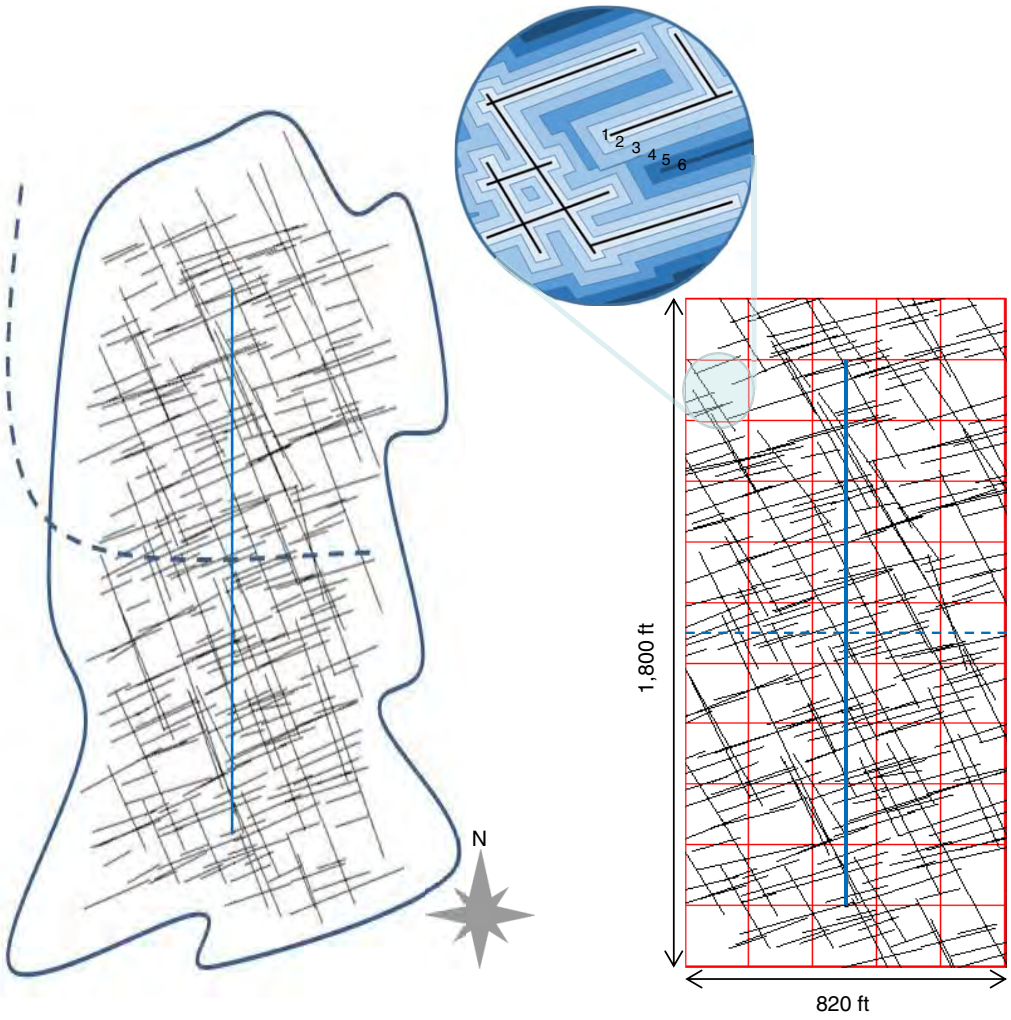

Fig. 23—Stimulated fracture network around a hydraulic fracture in the synthetic case.

To obtain a reference solution, very-fine-grid cells are used for the discretization of the matrix medium. All fractures are explicitly discretized. The flow exchange between a matrix cell and the fracture nodes is computed using the method described in Sarda et al. (2002). In the DP model and the EDFM-MINC approach, the reservoir domain is discretized by a $5 \times 11 \times 1$ uniform grid (Fig. 23). Different upscaling methods for the computation of equivalent fracture permeability in the homogenized medium are compared for a simulation of single-phase flow.

Simulation of Single-Phase Flow. First, we simulate a single-phase oil-production problem. The matrix permeability is 0.0001 md. Two fine-grid simulations are performed with 2.2 million and 8.8 million matrix cells, respectively, and compared in **Fig. 24.** These two simulations are very close, so we can consider them as the reference solution.

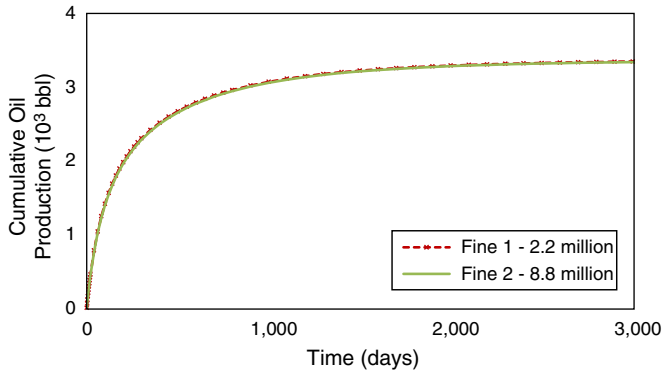

Fig. 24—Single-phase fine-grid simulations on the synthetic case.

It is well-known that homogenization of fractures is a sizable challenge, especially for the equivalent-permeability calculation. This study allows us to check our proposed EDFM-MINC approach as well as different upscaling methods.

Three upscaling techniques are used to compute equivalent permeabilities k_{eq}: an analytical method (Oda 1986), a local numerical method at the scale of a grid cell, and a global upscaling method. For the local upscaling method, because only a few fractures are contained in a grid cell, the cell cannot be considered as a representative elementary volume. Hence, the error on equivalent permeabilities may be large. The global upscaling method consists of applying the numerical method by imposing the boundary condition on the whole SRV to obtain an estimation of the equivalent permeability. In this example, the global volume contains more than 250 connected fractures, and it can be considered as a representative elementary volume. **Fig. 25** compares the EDFM-MINC8 simulation (a matrix cell is divided into eight subcells) using different equivalent permeabilities with the reference solution. As expected, the analytical method is not sufficiently accurate, and the local upscaling method is not accurate either because the volume of a grid cell is too small to be representative. The global upscaling method, which is a numerical approach on a representative elementary volume, provides a quite satisfactory result. Fig. 25 presents a DP simulation with the global upscaled permeability. This DP approach greatly underestimates the well performance and is not suitable for simulations of fractured low-permeability reservoirs.

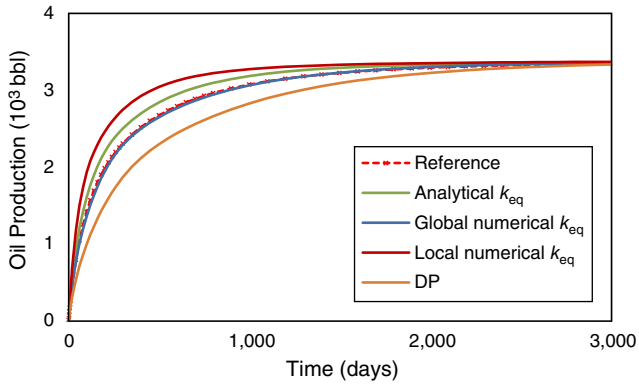

Fig. 25—Comparison of different upscaling models for the simulation of single-phase flow.

In the following subsections, the equivalent permeability obtained with the global upscaling method will be used for multiphase-flow simulations.

Tight Oil With Phase Change. Now, let us simulate the multiphase tight oil problem with a black-oil model. The matrix permeability is 0.0001 md. The initial reservoir pressure is 3,800 psi, and the bottomhole well flowing pressure is 1,160 psi. The bubblepoint pressure is 2,710 psi.

Initially, the reservoir is saturated with oil and mobile water. The rock is assumed to be water-wet. For the reference solution of this case, the matrix medium is discretized with 2.2 million cells. As shown by the previous test in a single matrix block, the use of a DP model is not appropriate to simulate flow phenomena related to phase changes, while the EDFM-MINC approach provides a satisfactory solution thanks to the fine-grid cells near the fracture faces. Such observations remain valid at the field scale, as shown later.

Fig. 26 compares the oil and gas production for different simulations (EDFM-MINC, DP, and the reference solution). Although some small differences are found among the EDFM-MINC methods, all the MINC simulations give reasonably accurate results compared with the reference solution, whereas the DP model greatly underestimates both the oil and gas production. **Fig. 27** shows the evolution of GOR—which is similar for all simulations, including the DP simulation—during a long period of approximately 7 years. In fact, the average homogenized fracture permeability is approximately 0.011 md, and permeability contrast between the homogenized fracture medium and the matrix medium is not very high, approximately 100 times. Therefore, the fluid transferred from the matrix to the fracture cannot be immediately produced by the well. Then, the pressure inside the fracture remains high, especially in the regions far from the well, and two-phase-flow phenomena caused by phase change inside the matrix is still limited in a small region. Therefore, the effect of matrix/fracture interaction on the phase change is not very significant. It has to be mentioned that our EDFM-MINC model does not take into account the exchange between a matrix cell and the fractures of neighboring cells. In addition, it is not very accurate if several matrix blocks with very different sizes are contained in a simulation cell, as discussed later. Therefore, it is not a surprise that the EDFM-MINC is less accurate on this synthetic case than on the single-block case presented previously.

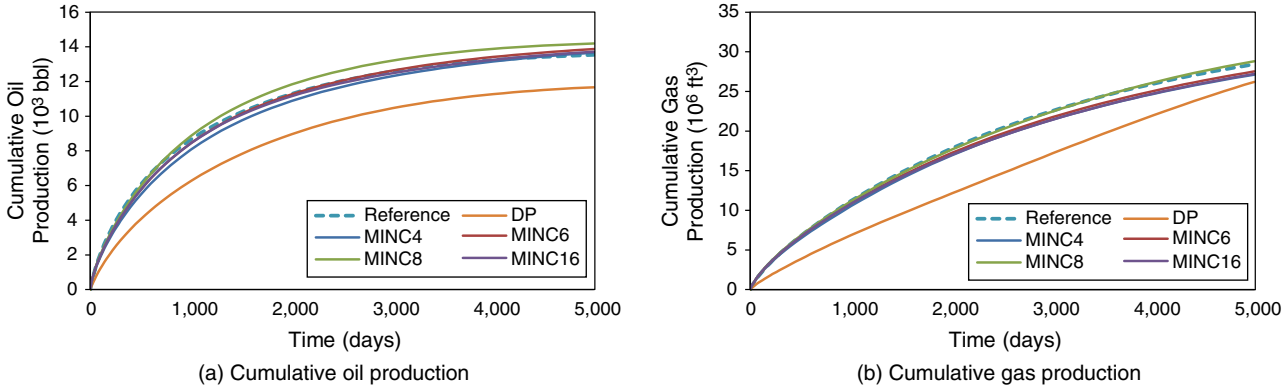

(a) Cumulative oil production

(b) Cumulative gas production

Fig. 26—Tight oil simulations in the synthetic reservoir with $k_m = 0.0001$ md.

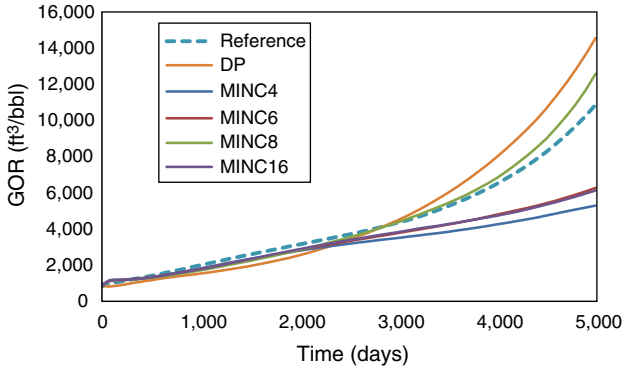

Fig. 27—GOR for the tight oil simulation with $k_m = 0.0001$ md.

Fig. 28 compares water production. At early times, the EDFM-MINC approach is close to the reference solution, thanks to their fine-grid cells near the fracture. Later, however, the EDFM-MINC approach fails to reproduce the reference solution, although it is still more predictive than the DP model. EDFM-MINC underestimates water production, whereas the DP model largely overestimates it. For this case, water production is relatively low compared with the oil rate, because of the high capillary retention of the rock that is both tight and water-wet.

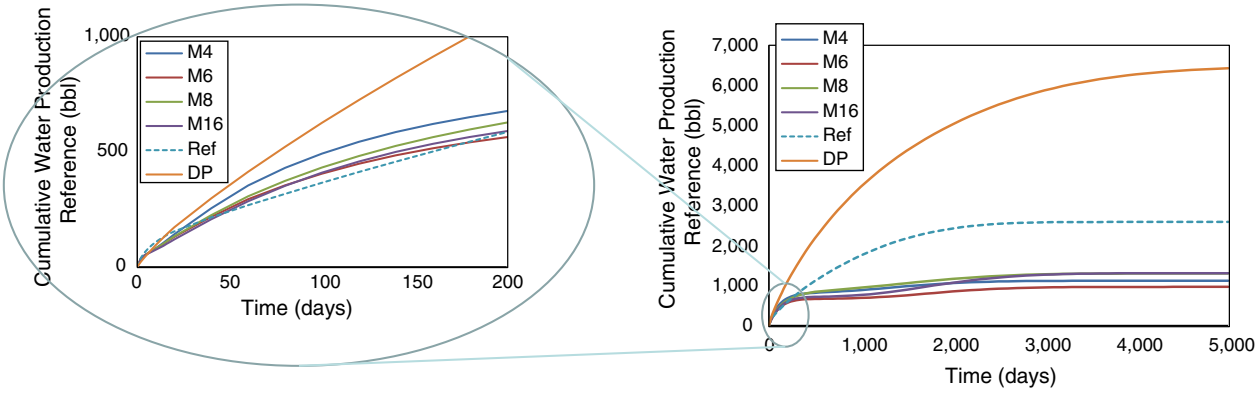

Fig. 28—Cumulative water production with $k_m = 0.0001$ md.

Now, we increase the fracture/matrix-permeability contrast and consider a matrix permeability of 0.00001 md. **Fig. 29** presents the daily oil/gas rates for this case. Again, all MINC simulations are accurate enough. The DP model greatly underestimates the oil rate during the first 2 years, and overestimates it later. For the gas production, the DP model underestimates it for more than 10 years. **Fig. 30** shows the GOR. In this test, the EDFM-MINC method simulates correctly the pressure drop and the phase change near the fractures, whereas the DP model delays the phase-change behavior in the near-fracture zone because of higher matrix pressure. **Fig. 31** presents the cumulative water production. In this extremely low-permeability case, the water production is satisfactorily simulated with the EDFM-MINC method.

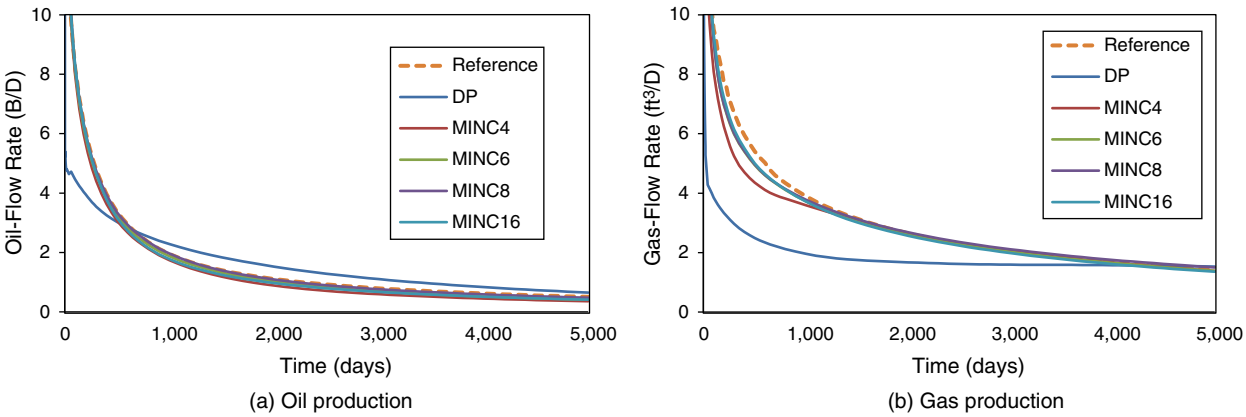

Fig. 29—Tight oil simulations with $k_m = 0.00001$ md.

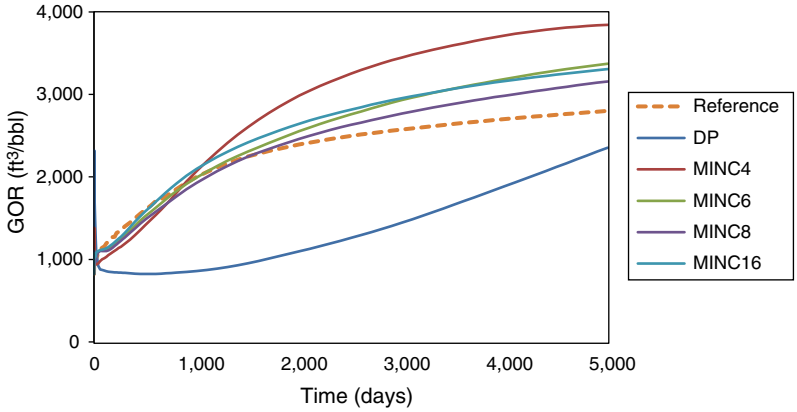

Fig. 30—GOR in the synthetic reservoir with $k_m = 0.00001$ md.

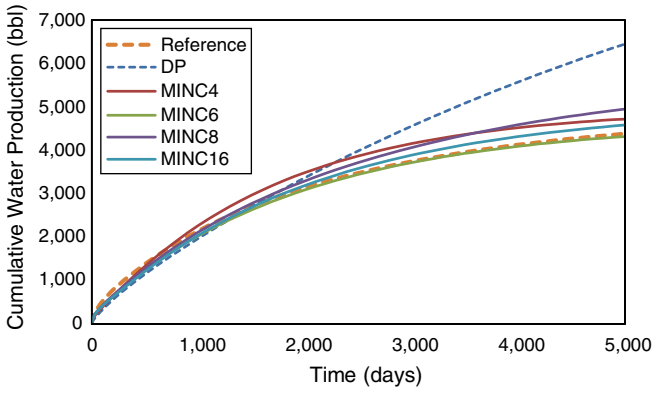

Fig. 31—Cumulative water production in the synthetic reservoir with $k_m = 0.00001$ md.

Shale Gas With Condensate. We consider a liquid-rich gas/condensate reservoir with a retrograde condensation issue. The gas composition is the same as in the single-matrix-block case presented previously (Table 2). The initial reservoir pressure is 6,000 psi, and the well BHP is 1,200 psi. The dewpoint pressure is approximately 3,000 psi. For this gas/condensate case, we encountered a numerical-convergence issue for the fine-grid simulation with 2.2 million matrix cells. That issue could not be investigated for lack of time, and hence the reference solution was obtained on a coarser model, with 550,000 matrix cells.

Fig. 32 compares gas and condensate production simulated with various EDFM-MINC models, the DP approach, and the reference solution. All MINC simulations are close to the reference solution. The DP model is not accurate, especially for the condensate simulation. **Fig. 33** shows the produced CGR from the well. The initial value of 0.00004 bbl/ft^3 corresponds to the condensate content of the reservoir fluid in its initial single-phase state. At very early times, the produced CGR starts to decrease because the pressure drops to less than the dewpoint pressure in the outer parts of matrix blocks near fractures, thus causing a condensate deposit that is preferentially retained there while reducing gas production from the matrix medium. This phenomenon is reproduced with the fine-grid simulation model (reference solution) and with the MINC method. However, when using a DP model, the CGR remains constant for more than 1 year because the pressure in the matrix cells remains higher than the dewpoint pressure during that initial period of production.

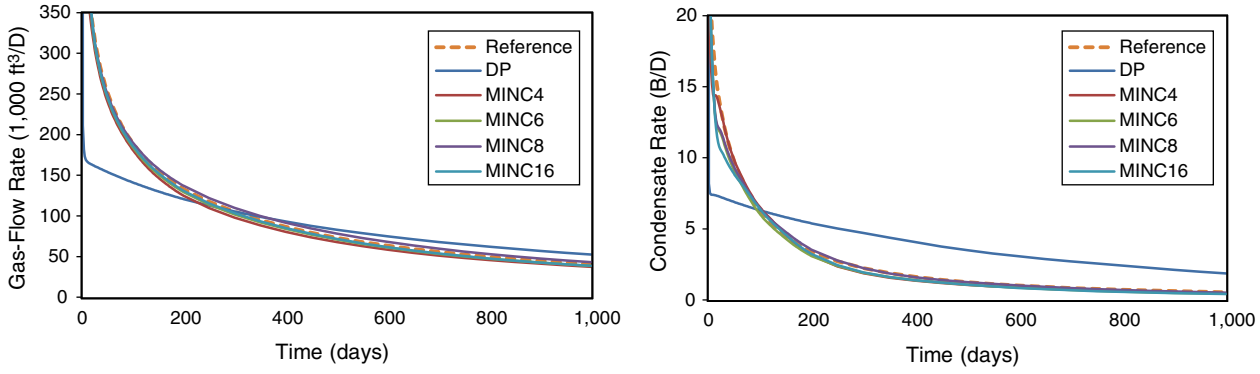

(a) Gas production rate

(b) Condensate production

Fig. 32—Gas/condensate reservoir in the synthetic case with $k_m = 0.00001$ md.

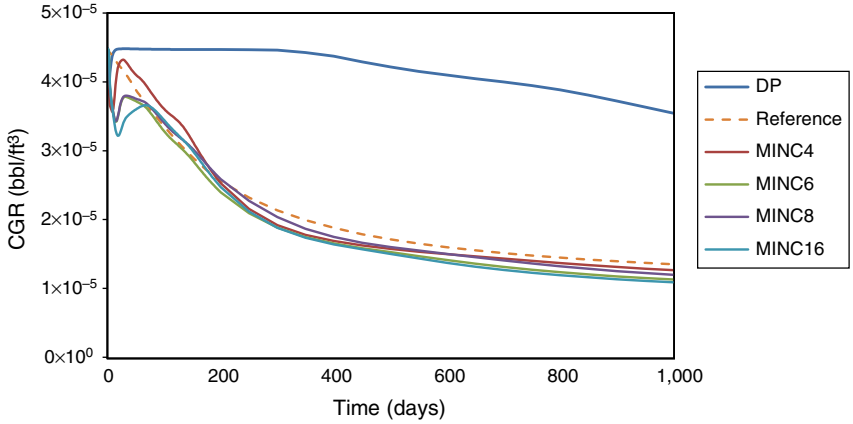

Fig. 33—CGR in the gas synthetic case.

From the simulation results, we also notice that although all MINC subdivisions provide globally satisfactory results, increasing the number of matrix subdivisions does not always ameliorate the accuracy. In fact, with complex physics, such as a multiphase flow with phase change, the simulation results and especially GOR are very sensitive to the grid sizes near the fractures. Besides, the MINC subdivisions are performed according the distance from the fractures, and this discretization does not always follow the isopressure lines when it goes far from the fractures. This kind of subdivision may also lead to a nonconvergence issue, although errors are small (Ding et al. 2014b; Cai et al. 2015). Moreover, no flow exchange is computed between two neighbor matrix cells if both of them contain fractures. With various block sizes present in a simulation cell, this method is also not very accurate, as discussed in the later section Discussion and Further Improvements. All these issues might lead to inaccurate simulation results and need to be improved. Nevertheless, we notice that the general trends are satisfactory for reservoir-simulation purposes.

Table 3 summarizes the CPU times for the EDFM-MINC and the fine-grid single-porosity simulations. Using the EDFM-MINC model, the CPU time is reduced from several hours to less than 1 minute.

	Explicit Discretized Model (Single Porosity)		Discrete-Fracture Model (MINC8)	
Case	No. of Grid Cells	CPU Time	No. of Grid Cells	CPU Time
Single-phase flow	2,200,624	5 hours	504	20 seconds
Tight oil three-phase flow		7 hours		30 seconds
Retrograde gas	550,624	30 hours		37 seconds

Table 3—Comparison of CPU time.

In summary, the EDFM-MINC method is successfully applied to the synthetic case, where two families of fractures are generated using a geostatistical model. In general, the MINC approach gives quite satisfactory results for both tight oil and shale-gas simulations, because of its ability to handle the phase-change effect on matrix/fracture interaction. The gain in CPU time is significant. Although this method is not always as accurate as the reference solution depending on the MINC subdivisions, the obtained results are much better than those from a DP simulation. On the other hand, the conventional DP model is not suitable for simulations of low-permeability reservoirs, whereas the EDFM-MINC approach greatly improves the accuracy. The EDFM-MINC provides a good compromise between simulation accuracy and efficiency in computational time.

Discussion and Further Improvements

It is well-known that a standard DP model cannot correctly simulate the matrix/fracture exchange because matrix blocks are not subgridded and because a single average block size is considered in DP cells containing several matrix blocks of different sizes. Previous simulation examples have shown that the MINC method can overcome the former limitation. The present section aims at demonstrating that the MINC method may also be a solution to take into account the nonuniform distribution of matrix block sizes at reservoir-simulation cell scale.

Modeling the matrix/fracture interaction for blocks of various sizes requires accounting for the fact that small blocks contribute only to the early stage of production, whereas large blocks contribute to both early and late stages. Regarding the EDFM-MINC model, the transmissibility formula given by Eq. 13 for the interporosity-flow calculation needs to be corrected. Otherwise, the matrix/fracture-exchange rate will be overestimated because the fluid in an inner subdivision of a large matrix block is driven to the fracture through larger exchange surfaces, which are the sum of the exchange surfaces of all the matrix blocks in the considered cell.

Fig. 34 shows an example of a simulation cell, sized 300×300 ft, surrounded by fractures and containing two orthogonal fractures inside. This cell is composed of four rectangular matrix blocks with sizes of 30×30 ft for block B_1, 30×270 ft for block B_2, 270×30 ft for block B_3, and 270×270 ft for block B_4. The fracture aperture and permeability are set at 0.004 ft and 2,500 md, respectively, and the matrix permeability is 0.0001 md. A single-phase gas-flow simulation is performed. **Fig. 35** presents a comparison of the MINC6 approach and the reference solution obtained with very-fine-grid cells. We observe that the MINC method is only accurate during the first 150 days, and that it overestimates the gas production afterward. The increasing inaccuracy of the MINC method at late times is related to the different sizes of the matrix blocks contained in the cell.

To illustrate the origin of this inaccuracy, **Fig. 36** plots the cumulative matrix volume vs. the distance from the fractures in each of the four matrix blocks as well as the total cumulative volume vs. the distance from fractures in the simulation cell (blue curve). This type of curve is the basis for calculating the matrix/fracture transmissivity in the MINC model, as formulated by Eqs. 13 and 14.

Clearly, the maximum distance found in block B_1 is the same as that in blocks B_2 and B_3, and the curves for B_2 and B_3 are the same. However, the maximum distance of exchange is much larger for block B_4, which is a large square block. For this reason, the matrix/fracture-flow transfer is completed after a much-longer time for that matrix block than for the other blocks. It has to be mentioned that the flow exchange between a matrix block and the fractures is limited in that matrix block. In other words, the exchange surface for the fluid in a block B_i should be calculated using the cumulative curve of the block B_i. However, the MINC transmissibilities determined from Eq. 13 are dependent on the total cumulative distribution curve, which corresponds to the sum of all the curves for a small distance from the fractures and to the curve from B_4 alone for large distances. Therefore, when the fluid from the center of B_4 is produced into the fractures, the exchange surface area is overestimated in the near-fracture zone because of the contribution from the small blocks in that surface area. This leads to an overestimation of the gas production at late times.

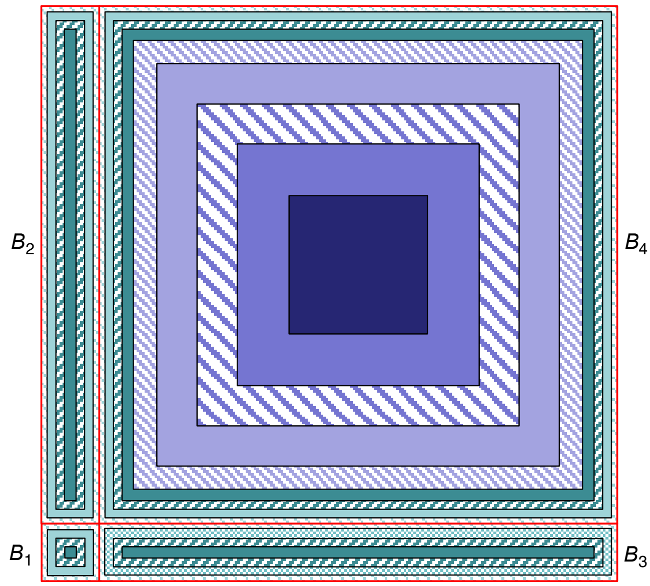

Fig. 34—MINC subdivision in a simulation cell containing four matrix blocks with different sizes.

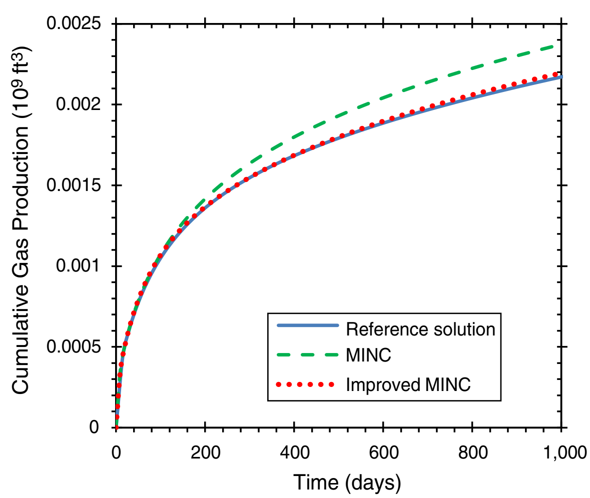

Fig. 35—Simulation results in a cell containing matrix blocks of different sizes.

To overcome this inaccuracy, we suggest modifying the transmissibility values when the contribution of a matrix subblock ends in the total cumulative distribution curve, to take into account only the producing blocks. In the example illustrated by Fig. 34, the exchange surface is calculated with all four subblocks when the distance is smaller than 15 ft, but has to be computed with the sole block B_4 when the distance is larger than 15 ft. To that end, the transmissibility $T_{i,i+1}$ between MINC subdivisions i and i+1 such that $d_i \leq 15 < d_{i+1}$ is corrected by the additional term $T'_{i,i+1}$ so that the flow from the subdivision (i+1) to the fracture under a steady-state regime corresponds to the transfer from block B_4 alone; that is,

$$\frac{1}{T'_{i,i+1}} + \sum_{j=0}^{i-1} \frac{1}{T_{j,j+1}} = \sum_{j=0}^{i} \frac{1}{T^4_{j,j+1}}, \quad \ldots \ldots (17)$$

where $T_{j,j+1}$ ($j = 0, 1, \ldots, i$–1) is the transmissibility calculated by Eq. 13 using the total cumulative distribution function, and $T^4_{j,j+1}$ is the transmissibility calculated with the cumulative distribution of only block B_4.

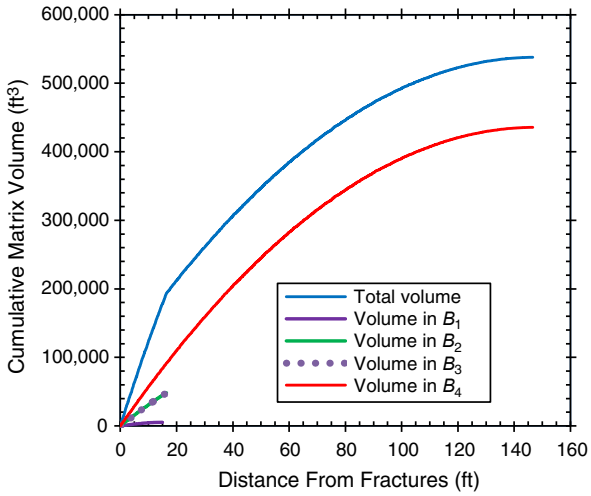

Fig. 36—Cumulative volume vs. distance for blocks of different sizes.

Fig. 35 also presents the simulation with the MINC6 approach using the modified transmissibility. With the corrected transmissibility, the result is greatly improved.

We have shown that it is possible to use an appropriate MINC approach to handle the matrix/fracture interaction for a simple distribution of blocks of different sizes. How to handle this issue of matrix/fracture interaction with various block sizes in the context of the DFN is our ongoing work.

It has to be mentioned that all presented examples are limited to two dimensions. Simulation with a 3D complex-fracture network, where the fractures can be oblique and/or the fractures are not fully penetrating the whole reservoir thickness and their heights are delimited by the stratabounds, is still a challenging issue. In that case, vertical communications cannot be easily handled using a simple MINC method because the fracture traces at the interface between the coarse simulation cells from one side to another might be completely different. Further studies are needed.

Conclusions

Unconventional shale-gas or tight oil reservoirs are characterized by multiscale fractures of various sizes embedded in extremely low-permeability formations, which increases the complexity of the reservoir simulation. A single-porosity model with explicitly discretized fractures is accurate for flow simulation, but it takes too much CPU time and is almost infeasible for field applications. A standard DP model is not accurate because of the extremely long transient period in matrix/fracture interaction caused by the ultralow permeability of the matrix medium and the nonlinear evolution of pressure inside the matrix blocks. To handle multiscale fracture networks, one solution is the EDFM approach, but it is still necessary to correctly treat the interactions between different media.

In this paper, we present an EDFM-MINC approach to simulate shale reservoirs. We also propose several techniques to ameliorate transmissibility computations for flow exchanges between the various media of an EDFM. Fractures are classified according to their conductivities. Hydraulic and propped fractures are explicitly discretized, and all other fractures, including stimulated and nonstimulated natural fractures, are homogenized. For matrix/fracture interaction, an MINC proximity function is used to subdivide the matrix medium to treat the matrix/fracture-flow exchange in a fully transient way. In this EDFM-MINC approach, equivalent permeability and porosity values are determined for the low-conductivity fractures only, whereas the matrix/fracture exchange involves all sorts of fractures with the MINC method. Moreover, the transmissibility computation between the explicitly discretized fracture and the homogenized medium can be improved by taking into account the pressure distribution using an integral method. A transmissibility formula between SRV and non-SRV zones associated to the MINC method is also derived.

The proposed EDFM-MINC approach is tested in two dimensions on both single-phase and multiphase flow with phase change in the presence of DFNs. This method provides quite satisfactory results, compared with the fine-grid single-porosity simulation with an explicit discretization of fractures. It can be used to simulate tight oil reservoirs as well as gas/condensate ones. Moreover, this method significantly reduces the number of grid cells, leading to a decrease in the CPU time compared with the single-porosity model. The EDFM-MINC offers a computationally efficient approach for simulating fluid flow in fractured low-permeability reservoirs, and provides a middle-ground solution between simulation accuracy and CPU time.

This promising EDFM-MINC approach calls for further development to take into account the distribution of matrix blocks at the scale of reservoir cells. How to efficiently handle this kind of problem is our ongoing work.

Nomenclature

a = matrix-block dimension, L
A = exchange area, L^2
b = matrix-block dimension, L
C = mole fraction
d = distance, L
F = flux, L^3T^{-1}
g = gravitational acceleration, LT^{-2}
J = diffusion/dispersion term, $mol \cdot L^{-2}T^{-1}$
k = absolute permeability, L^2
k_r = relative permeability

P = pressure, $ML^{-1}T^{-2}$
q = source/sink term, $L^3L^{-3}T^{-1}$ or T^{-1}
Q^{mf} = matrix/fracture-exchange term, $mol \cdot L^{-3}T^{-1}$
S = fluid saturation
t = time, T
T = transmissibility, L^3
$\vec{u}$ = velocity, LT^{-1}
v_{sg} = gas-sorption term, $mol \cdot L^{-3}$
V = volume, L^3
Z = depth, L
λ_p = mobility of phase p, $M^{-1}LT$
μ = viscosity, $ML^{-1}T^{-1}$
ρ = mole density, $mol \cdot L^{-3}$
σ = shape factor, L^{-2}
ς = cumulative frequency
ϕ = effective porosity of formation
Φ = flow potential, $ML^{-1}T^{-2}$

Superscripts

f = fracture
F = high-conductivity fracture
m = matrix
M = medium, fracture or matrix

Subscripts

c = component
f = fracture
g = gas
i = cell index
j = cell or node index
k = cell index
m = matrix
o = oil
p = phase
w = water

Acknowledgments

The authors gratefully acknowledge IFP Energies Nouvelles for their support.

References

Bourbiaux, B., Granet, S., Landereau, P. et al. 1999. Scaling Up Matrix-Fracture Transfers in Dual-Porosity Models: Theory and Application. Presented at the SPE Annual Technical Conference and Exhibition, Houston, 3–6 October. SPE-56557-MS. https://doi.org/10.2118/56557-MS.

Cai, L., Ding, D. Y., Wang, C. et al. 2015. Accurate and Efficient Simulation of Fracture–Matrix Interaction in Shale Gas Reservoirs. *Transport Porous Med.* **107** (2): 305–320. https://doi.org/10.1007/s11242-014-0437-x.

Delorme, M., Daniel, J. M., Kada-Kloucha, C. et al. 2013. An Efficient Model to Simulate Reservoir Stimulation and Induced Microseismic Events on 3D Discrete Fracture Network for Unconventional Reservoirs. Presented at the Unconventional Resources Technology Conference, Denver, 12–14 August. URTEC-1578312-MS.

Ding, D. Y., Wu, Y.-S. and Jeannin, L. 2014a. Efficient Simulation of Hydraulic Fractured Wells in Unconventional Reservoirs. *J. Pet. Sci. Eng.* **122** (October): 631–642. https://doi.org/10.1016/j.petrol.2014.09.005.

Ding, D. Y., Wu, Y.-S., Farah, N. et al. 2014b. Numerical Simulation of Low Permeability Unconventional Gas Reservoirs. Presented at the SPE/EAGE European Unconventional Resources Conference and Exhibition, Vienna, Austria, 25–27 February. SPE-167711-MS. https://doi.org/10.2118/167711-MS.

Famy, C., Bourbiaux, B. and Quintard, M. 2005. Accurate Modeling of Matrix-Fracture Transfers in Dual-Porosity Models: Optimal Subgridding of Matrix Blocks. Presented at the SPE Reservoir Simulation Symposium, Houston, 31 January–2 February. SPE-93115-MS. https://doi.org/10.2118/93115-MS.

Farah, N. and Ding, D. Y. 2016. Discrete Fracture Model Based on Multiple Interacting Continua Proximity Function for Unconventional Low Permeability Reservoir Simulations. Oral presentation given at ECMOR XV: 15th European Conference on the Mathematics of Oil Recovery, Amsterdam, 29 August–1 September.

Farah, N., Ding, D. Y., and Wu, Y. S. 2015. Simulation of the Impact of Fracturing Fluid Induced Formation Damage in Shale Gas Reservoirs. Presented at the SPE Reservoir Simulation Symposium, Houston, 23–25 February. SPE-173264-MS. https://doi.org/10.2118/173264-MS.

Farhadinia, M. A. and Delshad, M. 2010. Modeling and Assessment of Wettability Alteration Processes in Fractured Carbonates Using Dual Porosity and Discrete Fracture Approaches. Presented at the SPE Improved Oil Recovery Symposium, Tulsa, 24–28 April. SPE-129749-MS. https://doi.org/10.2118/129749-MS.

Fourno, A., Noetinger, B., and Borderie C. 2016. An Original and Useful Approach to Mesh a Discrete Fracture Network Using a Delaunay Triangulation: Application on Flow and Transport Upscaling From Characterization Scale to Reservoir Scale. Oral presentation given at Computational Methods in Water Resources (CMWR) XXI International Conference, Toronto, Canada, 20–24 June.

Fumagalli, A., Pasquale, L., Zonca, S. et al. 2016. An Upscaling Procedure for Fractured Reservoirs With Embedded Grids. *Water Resour. Res.* **52** (8): 6506–6525. https://doi.org/10.1002/2015WR017729.

Gong, B., Karimi-Fard, M., and Durlofsky, L. J. 2006. An Upscaling Procedure for Constructing Generalized Dual-Porosity/Dual-Permeability Models from Discrete Fracture Characterizations. Presented at the SPE Annual Technical Conference and Exhibition, San Antonio, Texas, 24–27 September. SPE-102491-MS. https://doi.org/10.2118/102491-MS.

Hajibeygi, H., Karvounis, D., and Jenny, P. 2011. A Hierarchical Fracture Model for the Iterative Multi-Scale Finite Volume Method. *J. Comput. Phys.* **230** (24): 8729–8743. https://doi.org/10.1016/j.jcp.2011.08.021.

Hyman, J. D., Karra, S., Makedonska, N. et al. 2015. DFNWorks: A Discrete Fracture Network Framework for Modeling Subsurface Flow and Transport. *Comput. Geosci.* **84** (November): 10–19. https://doi.org/10.1016/j.cageo.2015.08.001.

Jiang, J. and Younis, R. M. 2016. Hybrid Coupled Discrete-Fracture/Matrix and Multicontinuum Models for Unconventional-Reservoir Simulation. *SPE J.* **21** (3): 1009–1027. SPE-178430-PA. https://doi.org/10.2118/178430-PA.

Jiang, J., Shao, Y., and Younis, R. M. 2014. Development of a Multi-Continuum Multi-Component Model for Enhanced Gas Recovery and CO_2 Storage in Fractured Shale Gas Reservoirs. Presented at the SPE Improved Oil Recovery Symposium, Tulsa, 12–16 April. SPE-169114-MS. https://doi.org/10.2118/169114-MS.

Karimi-Fard, M., Durlofsky, L. J., and Aziz, K. 2004. An Efficient Discrete-Fracture Model Applicable for General-Purpose Reservoir Simulators. *SPE J.* **9** (2): 227–236. SPE-88812-PA. https://doi.org/10.2118/88812-PA.

Khvoenkova, N. and Delorme, M. 2011. An Optimal Method to Model Transient Flows in 3D Discrete Fracture Network. Oral presentation given at IAMG 2011, Salzburg, Austria, 5–9 September.

Khvoenkova, N., Bossie-Codreanu, D., Broussard, N. et al. 2015. Application of the DDFN (Discrete and Deformable Fracture Network) Method Within an Integrated Unconventional Reservoir Study Workflow. Presented at the SPE Annual Technical Conference and Exhibition, Houston, 28–30 September. SPE-175112-MS. https://doi.org/10.2118/175112-MS.

Lee, S. H., Lough, M. F., and Jensen, C. L. 2001. Hierarchical Modelling of Flow in Naturally Fractured Formations With Multiple Length Scale. *Water Resour. Res.* **37** (3): 443–445. https://doi.org/10.1029/2000WR900340.

Li, L. and Lee, S. H. 2008. Efficient Field-Scale Simulation of Black Oil in a Naturally Fractured Reservoir Through Discrete Fracture Networks and Homogenized Media. *SPE Res Eval & Eng* **11** (4): 750–758. SPE-103901-PA. https://doi.org/10.2118/103901-PA.

Lim, K. T. and Aziz, K. 1995. Matrix-Fracture Transfer Shape Factors for Dual-Porosity Simulators. *J. Pet. Sci. Eng.* **13** (3–4): 169–178. https://doi.org/10.1016/0920-4105(95)00010-F.

Matthäi, S. K., Menzentsev, A., and Belayneh, M. 2005. Control-Volume Finite-Element Two-Phase Flow Experiments With Fractured Rock Represented by Unstructured 3D Hybrid Meshes. Presented at the SPE Reservoir Simulation Symposium, Houston, 31 January–2 February. SPE-93341-MS. https://doi.org/10.2118/93341-MS.

Mirzaei, M. and Cipolla, C. L. 2012. A Workflow for Modelling and Simulation of Hydraulic Fractures in Unconventional Gas Reservoirs. Presented at the SPE Middle East Unconventional Gas Conference and Exhibition, Abu Dhabi, 23–25 January. SPE-153022-MS. https://doi.org/10.2118/153022-MS.

Moinfar, A., Narr, W., Hui, M. H. et al. 2011. Comparison of Discrete-Fracture and Dual-Permeability Models for Multiphase Flow in Naturally Fractured Reservoirs. Presented at the SPE Reservoir Simulation Symposium, The Woodlands, Texas, 21–23 February. SPE-142295-MS. https://doi.org/10.2118/142295-MS.

Moinfar, A., Varavei, A., Sepehnoori, K. et al. 2013. Development of a Coupled Dual Continuum and Discrete Fracture Model for the Simulation of Unconventional Reservoirs. Presented at the SPE Reservoir Simulation Symposium, The Woodlands, Texas, 18–20 February. SPE-163647-MS. https://doi.org/10.2118/163647-MS.

Norbeck, J., Huang, H., Podgorney, R. et al. 2014. An Integrated Discrete Fracture Model for Description of Dynamic Behavior in Fractured Reservoirs. Oral presentation of paper SGP-TR-202 given at the Thirty-Ninth Workshop on Geothermal Reservoir Engineering, Stanford University, Stanford, California, 24-26 February.

Oda, M. 1986. Permeability Tensor for Discontinuous Rock Masses. *Geotechnique* **35** (4): 483–495. https://doi.org/10.1680/geot.1985.35.4.483.

Pruess, K. and Karasaki, K. 1982. Proximity Functions for Modeling Fluid Flow and Heat Flow in Reservoirs With Stochastic Fracture Distributions. *Proc.,* Eighth Workshop on Geothermal Reservoir Engineering, Stanford University, Stanford, California, December, 219–224.

Pruess, K. and Narasimhan, T. N. 1985. A Practical Method for Modeling Fluid and Heat Flow in Fractured Porous Media. *SPE J.* **25** (1): 14–26. SPE-10509-PA. https://doi.org/10.2118/10509-PA.

Sarda, S., Jeannin, L., Basquet, R. et al. 2002. Hydraulic Characterization of Fractured Reservoirs: Simulation on Discrete Fracture Models. *SPE Res Eval & Eng* **5** (2): 154–162. SPE-77300-PA. https://doi.org/10.2118/77300-PA.

Warren, J. E. and Root, P. J. 1963. The Behavior of Naturally Fractured Reservoirs. *SPE J.* **3** (3): 245–255. SPE-426-PA. https://doi.org/10.2118/426-PA.

Wu, Y.-S. and Pruess, K. 1988. A Multiple-Porosity Method for Simulation of Naturally Fractured Petroleum Reservoirs. *SPE Res Eval & Eng* **3** (1): 327–336. SPE-15129-PA. https://doi.org/10.2118/15129-PA.

Wu, Y. S., Li, J., Ding, D. et al. 2014. A Generalized Framework Model for the Simulation of Gas Production in Unconventional Gas Reservoirs. *SPE J.* **19** (5): 845–857. SPE-163609-PA. https://doi.org/10.2118/163609-PA.

Xu, Y., Cavalcante Filho, J. S. A., Yu, W. et al. 2016. Discrete-Fracture Modeling of Complex Hydraulic-Fracture Geometries in Reservoir Simulators. *SPE Res Eval & Eng* **20** (2): 1–20. SPE-183647-PA. https://doi.org/10.2118/183647-PA.

Didier Yu Ding is a senior research engineer in the Geosciences Division of IFP Energies Nouvelles (IFPEN). His research interests include reservoir simulation and characterization, numerical modeling, and unconventional hydrocarbon reservoirs. Ding holds a bachelor's degree in mathematics from Peking University, China, and master's and PhD degrees in applied mathematics from the University of Paris.

Nicolas Farah was a PhD degree candidate at IFPEN and now works at Lebanese American University. His research interests include reservoir simulation and characterization, especially for unconventional hydrocarbon reservoirs. Farah holds a bachelor's degree in physics from Lebanese University, a master's degree in petroleum engineering from UPPA University, France, and a PhD degree in geosciences from the University of Paris.

Bernard Bourbiaux is a research engineer in the Geosciences Division of IFPEN. He has been with IFPEN for more than 30 years. Bourbiaux's research interests include multiphase transfers in porous media, fractured-reservoir modeling, and enhanced oil recovery. He holds an engineering degree from École Nationale Supérieure de Géologie, France, and a master's degree in reservoir management from IFP School, France.

Yu-Shu Wu is a professor, holder of the Foundation CMG Reservoir Modeling Chair, and the director of Energy Modeling Group Research Center in the Petroleum Engineering Department at the Colorado School of Mines. Previously, he was a staff scientist

with the Earth Sciences Division of Lawrence Berkeley National Laboratory for 14 years (1995–2008). At the Colorado School of Mines, Wu teaches and performs research in reservoir engineering, multiphase fluid and heat flow, geomechanics, unconventional oil and gas reservoir dynamics, carbon dioxide geosequestration and enhanced oil recovery, geothermal engineering, and numerical reservoir simulation. He is a fellow of the Geological Society of America.

Imen Mestiri is an energy engineer. Her research interests include optimization, phase-behavior calculations, renewable-energy-grid integration, and energy-saving measures. Mestiri holds an engineering degree from École Polytechnique of Tunisia and a master's degree in energy economics from IFP School. She is a member of SPE.